Lehigh University
Lehigh Preserve

Fritz Laboratory Reports | Civil and Environmental Engineering

1980

Local buckling of cylindrical tubular columns made of a-36 steel, February 1980 61p

Alexis Ostapenko

David F. Grimm

Follow this and additional works at: http://preserve.lehigh.edu/engr-civil-environmental-fritz-lab-reports

Recommended Citation
Ostapenko, Alexis and Grimm, David F., "Local buckling of cylindrical tubular columns made of a-36 steel, February 1980 61p" (1980). *Fritz Laboratory Reports.* Paper 2234.
http://preserve.lehigh.edu/engr-civil-environmental-fritz-lab-reports/2234

This Technical Report is brought to you for free and open access by the Civil and Environmental Engineering at Lehigh Preserve. It has been accepted for inclusion in Fritz Laboratory Reports by an authorized administrator of Lehigh Preserve. For more information, please contact preserve@lehigh.edu.

LOCAL BUCKLING OF CYLINDRICAL TUBULAR COLUMNS

MADE OF A-36 STEEL

by

Alexis Ostapenko

David F. Grimm

This research was sponsored by the
American Petroleum Institute as
PRAC Project No. 16.

Fritz Engineering Laboratory Report No. 450.7

Lehigh University, Bethlehem, Pa.

February 1980

TABLE OF CONTENTS

	Page
ABSTRACT	
1. INTRODUCTION	
1.1 Background	1
1.2 Previous Research at Lehigh University	2
1.3 Objectives of Present Research	2
2. DESCRIPTION OF THE TEST SPECIMENS	
2.1 Geometric Parameters	3
2.2 Material Properties	3
2.3 Fabrication Process	6
3. INITIAL GEOMETRIC IMPERFECTIONS	
3.1 Standard Imperfections	7
3.1.1 Definitions and Methods of Measurement	7
3.1.2 Discussion of Imperfections	8
3.1.3 Comparison with API Recommendations	9
3.2 Initial Shape	9
3.3 Local Imperfections	10
4. RESIDUAL STRESSES	
4.1 General	11
4.2 Method of Measurement	11
4.3 Discussion of Residual Stresses	12
5. TEST PROCEDURE	
5.1 Test Setup	15
5.2 Instrumentation	15
5.3 Test Sequence	16

Page

6. TEST RESULTS

6.1 General Specimen Behavior 18

6.1.1 Prebuckling Behavior 18
6.1.2 Behavior at Buckling 20
6.1.3 Post-Buckling Behavior 21

6.2 Behavior of Individual Specimens 22

6.2.1 Behavior of Specimen T1 22
6.2.2 Behavior of Specimen T2 23
6.2.3 Behavior of Specimen T3 24
6.2.4 Behavior of Specimen T4 25
6.2.5 Behavior of Specimen T5 26
6.2.6 Behavior of Specimen P11 27

7. DISCUSSION OF TEST RESULTS

7.1 General Specimen Behavior 28

7.1.1 Prebuckling Behavior 28
7.1.2 Behavior at Buckling 30
7.1.3 Post-Buckling Behavior 31

7.2 Comparison of Specimen Behavior 31

7.2.1 Comparison of Specimens T1 and T5 31
7.2.2 Comparison of Specimens T2, T3, and T4 32
7.2.3 Comparison of Specimens P11 and P9 33

7.3 Effect of Initial Imperfections 33

7.4 Effect of Residual Stresses 34

7.5 Effect of D/t Ratio 35

7.6 Effect of α and c 35

7.7 Comparison of Test Results with Design Curves 37

8. SUMMARY AND CONCLUSIONS 39

9. RECOMMENDATIONS 42

10. ACKNOWLEDGMENTS 43

11. NOMENCLATURE 44

12. REFERENCES 45

LOCAL BUCKLING OF CYLINDRICAL TUBULAR COLUMNS MADE OF A-36 STEEL

by

Alexis Ostapenko
David F. Grimm

ABSTRACT

To investigate the effect of the yield stress on the local buckling of tubular columns fabricated by cold-rolling and welding, tests were conducted on five specimens made of ASTM A-36 steel (nominal yield stress 250 MPa (36 ksi)) and on one made of ASTM A-514 steel (nominal yield stress 700 MPa (100 ksi)). The wall thickness varied from 6.55 to 9.73 mm (0.26 to 0.38 in.) and the diameter-to-thickness ratio (D/t) from 59 to 233. The slenderness ratio (L/r) was less than 9 to preclude the effect of overall column buckling.

The ultimate stress was limited by the formation of local buckles in four of the specimens. In the remaining two, stresses were reached slightly above those at which buckling was observed. The buckling stresses ranged from 0.829 to 1.069 of the static yield stress and generally decreased with an increase in D/t ratio.

The initial geometric imperfections and the longitudinal welding residual stresses appeared to have no influence on either the location or the pattern of the local buckles. In the post-buckling range the specimens were able to maintain capacities of 12 to 23% of their buckling strength.

The test results were compared using several design parameters and equations. Current American design equations were all found to be conservative. An equation was proposed to predict the local buckling strength of cylindrical tubular columns fabricated from steels with a static yield stress of 250 MPa (36 ksi) to 700 MPa (100 ksi).

1. INTRODUCTION

1.1 Background

The symmetry of a cylindrical tubular member permits it to be efficiently used to resist the three-dimensional loadings that occur in structures such as offshore platforms, elevated storage tanks and transmission towers. When these members are subjected to compression, one of the possible failure mechanisms is that of local buckling. Yet, despite its importance as a design parameter, there are no methods currently available for accurately predicting the local buckling strength.

There is considerable disagreement among various local buckling theories and generally poor correlation between these theories and the relatively sparse test results (1,2,3,4). Many of the theories are based on tests conducted principally on small tubes of various materials manufactured by extrusion, electric resistance welding, and other manufacturing processes. On the other hand, the large cylindrical members currently used in many structures are usually made of steel and fabricated by cold-rolling and welding which generally results in more severe imperfections and higher residual stresses than in the manufacturing processes (1,2). The local buckling of these members was believed to be particularly influenced by their size, material and the production process. As only a small number of test results for cylinders with relatively low yield stress levels was available, there was an evident need for more accurate local buckling criteria for fabricated high strength members.

1.2 Previous Research at Lehigh University

In order to gain a better understanding of local buckling of fabricated high-strength steel cylindrical columns, eleven specimens were tested in a research program supported by AISI at Lehigh University (5,6,7). Very consistent correlation was obtained among the ten test results from the specimens made of steel with a yield stress of 350 MPa (50 ksi) and an equation was developed for predicting the local buckling stress (4). However, a test on a 700 MPa (100 ksi) specimen gave a significantly higher local buckling stress than indicated by this equation. This fact pointed to the possibility that cylindrical columns with a yield stress lower than 350 MPa (50 ksi), such as 250 MPa (36 ksi) may have a substantially lower local buckling stress than would be predicted by this equation.

1.3 Objectives of Present Research

The objective of the research described herein was to investigate the local buckling strength of cylindrical tubular columns fabricated from ASTM A36 steel (8) with a nominal yield stress of 250 MPa (36 ksi) and to propose a suitable local buckling design method. Two areas of particular interest were whether the design equation proposed in Ref. 4 could also be applied to members made of 250 MPa (36 ksi) steel, and whether the consistency observed in the test results of Refs. 5, 6 and 7 could also be achieved for the 250 MPa (36 ksi) specimens since the test results for this steel reported by other researchers showed considerable scatter (9,10).

An additional objective was to validate the previous test result on the 700 MPa (100 ksi) specimen (4) by retesting the old specimen.

2. DESCRIPTION OF THE TEST SPECIMENS

2.1 Geometric Parameters

The dimensions and other physical parameters of the cylindrical specimens are listed in Tables 1 (SI units) and 1A (English units). The outside diameters ranged from 0.58 m (23.02 in.) to 1.53 m (60.30 in.) and the thicknesses from 2.02 mm (0.080 in.) to 9.94 mm (0.391 in.). The diameter-to-thickness ratios (D/t) ranged from 59 to 294. The length-to-radius of gyration ratios (L/r) of the specimens were less than 9.0 in order to preclude the effect of overall column buckling.

2.2 Material Properties

Specimens T1 to T5 were fabricated from ASTM A36 steel plate with a nominal yield stress of 250 MPa (36 ksi) (8). The intent of the project that the mill test results should deviate no more than 10% from the ASTM nominal yield stress was maintained for Specimens T1 to T4. However, the plate for Specimen T5 was taken from the fabricator's stockyard, and its yield stress was substantially higher. Specimen P11, donated to AISI, was fabricated from ASTM A514 Type B steel with a nominal yield stress of 700 MPa (100 ksi).

Static yield stress has been found to be the most consistent and reliable material property for analyzing the results of tests on steel structures and components. The procedure for determining the static yield stress is as follows. Shortly upon reaching the flattened portion of the stress-strain curve, that is, upon reaching the yield stress, the machine

head is stopped* and the load is allowed to stabilize within three to five minutes at a lower level. The resumption of straining leads to an increase of the load to a level dependent on the strain rate. At least two more stops are made within the plateau of yielding as shown in Fig. 1. The average of the reduced stresses at the bottoms of the dips is defined as the static yield stress, that is, the stress at a zero strain rate. After this, the coupon test proceeds in the usual manner (12)

The static yield stress for each specimen is given in Column 3 of Tables 1 and 1A. The yield stresses for Specimens T1 to T5 were obtained as the average of six or seven standard eight-inch gage length tensile coupons of each thickness cut in the longitudinal direction of the specimens. One set of three or four coupons of each plate thickness was tested at Lehigh University, and the second set was tested at Chicago Bridge & Iron Company (CB&I). For the 9.94 mm (3/8 in.) plate used in Specimen T1, the average static yield stress was 239 MPa (34.67 ksi) and the dynamic yield stress was 265 MPa (38.50 ksi). For the 6.73 mm (1/4 in.) plate used in Specimens T2, T3 and T4, the static yield stress was 204 MPa (29.56 ksi) and the dynamic was 239 MPa (34.67 ksi). These dynamic yield stresses were determined at a strain rate of 1042 μm/m/sec (1/16 in./in./min). This rate is the maximum testing rate permitted by ASTM A370 (11) and is commonly used by steel producers for determining mechanical properties given in mill test reports. The term nominal yield stress used in this report is the minimum specified yield stress on a tension specimen strained at rates up to the maximum permitted by ASTM A370(11).

---

* In a screw type machine, rotation of the screws is stopped: in a hydraulic machine, the valve is carefully controlled so that a dial gage, placed between the machine head and the base indicates no relative motions of the head.

The yield stresses for Specimen T5 were determined as the average of seven standard eight-inch gage length tensile coupons cut in the longitudinal direction of the specimen. The static yield stress was 336 MPa (48.67 ksi) and the dynamic was 362 MPa (52.5 ksi) at a testing rate of 1042 μm/m/sec.

Even though a rather large range existed among the yield stresses determined in the three A36 steel plates, the variation in a given plate at a given testing rate was small. The maximum difference in the static yield stress for the 9.94 mm (0.391 in.) plate was 14.9 MPa (2.16 ksi), or 6.2% of the average static yield stress. The static yield stress and the dynamic yield stresses at two different crosshead speeds are listed for individual coupons in Tables 2 and 2A.

For the 6.73 mm (0.265 in.) plate (Specimens T2, T3 and T4) an increase of 10% existed between the static and dynamic yield stresses determined at a crosshead speed of 52 μm/m/sec. An increase of 17% was between the static and dynamic yield stresses was determined at a maximum ASTM rate of 1042 μm/m/sec. These yield stresses are about 4% higher than the increases predicted by the equations developed in Ref. 12. The effect of strain rate was not as severe in the 9.94 mm (0.391 in.) plate (Specimen T1) as the dynamic yield stress was 8% higher than the static at 52 μm/m/sec and 11% higher at 1042 μm/m/sec.

The material properties of Specimen P11 were assumed to be those of the original Specimen P9. The static yield stress was 623 MPa (90.32 ksi) and the dynamic was 645 MPa (93.60 ksi) at 52 μm/m/sec (7).

2.3 Fabrication Process

All of the specimens were formed into cylinders in a pyramid three-roll bending machine by repeatedly cold-rolling the plate to a smaller and smaller radius until the opposite edges met. In Specimens T1 to T4 the edges were joined with a two-pass butt weld made from one end of the specimen to the other by the automatic submerged-arc process. As welding caused a flattening of the wall in the vicinity of the weld, the specimens were re-rolled to restore circularity. To permit re-rolling, the excess weld material was ground off. After re-rolling, steel end rings 22 mm thick by 127 mm wide (7/8 in x 5 in.) were welded to the ends of the specimens.

In Specimen T5 most of the welding distortions were prevented by small struts which had been tack welded inside the specimen near the longitudinal joint. The edges were joined with a two-pass single-bevel weld made manually by the submerged-arc process. After welding, the struts were removed and the end rings added.

Specimen P11 was made from Specimen P9, which had been tested in a previous project sponsored by the AISI at Lehigh University (7). The length of the original specimen containing the buckles (approximately 0.5 m, or 19 in.) was removed by flame cutting. Some small portions of the buckles were expected to recover elastically and were not removed. However, they failed to fully straighten out and the remaining dents were partially straightened by preheating both sides of the specimen wall and hammering. Finally, the end ring was rewelded to the shortened end. The local imperfections which remained are discussed in Chapter 3.

3. INITIAL GEOMETRIC IMPERFECTIONS

3.1 Standard Imperfections

3.1.1 Definitions and Methods of Measurement

A standard measure of initial geometric imperfections in a tubular member is given by the out-of-roundness and the out-of-straightness. The out-of-roundness at any given cross section is defined by:

$$\text{OUT-OF-ROUNDNESS} = \frac{OD_{max} - OD_{min}}{OD} \qquad (1)$$

where OD_{max} and OD_{min} are the maximum and minimum outside diameters of the cross section and $\overline{OD}$ is the mean outside diameter. The outside diameters at each end of the specimen were determined by placing the specimen within a reference circle drawn on the floor and measuring the distances between the reference circle and the specimen wall at the grid lines. (For example, Figure 2 shows the location of the grid lines for Specimen T5). The mean diameter was computed from the average of the measured circumferences at each end of the specimen. The out-of-roundness of other cross sections was determined from the end diameters and the offsets between the specimen wall and straight lines connecting the grid points on the end circumferences.

The out-of-straightness is defined by the maximum offset between a longitudinal straight line and the specimen wall in any 1.5 m (5 ft) length. The measurements were taken with a dial gage rig, and the offsets were determined as the differences between reference readings taken against a flat surface and the initial readings taken on the specimen.

3.1.2 Discussion of Imperfections

A summary of the out-of-roundness and out-of-straigthness measurements on each specimen is given in Tables 3 and 3A. The largest difference between the maximum and minimum outside diameters in the A36 specimens was 11.7 mm (0.46 in.) in Specimen T4. Specimen T5 was the most out-of-round at 0.0132, and T2 deviated the most from straightness with an initial inward deflection of 3.05 mm (0.120 in.)

Figs. 2 and 40 show the cross sections of Specimens T5 and T4 where the maximum imperfections were measured. The imperfections at the cross section near the location where the buckling occurred in each specimen are shown in Figs. 37 to 42. In these figures the reference circle is shown by the light dashed lines and the initial shape by the solid dark line. The offsets between the two shapes are the initial deviations magnified by a factor of 10.

Specimen P11 had the largest difference between diameters in any specimen with 18.3 mm (0.72 in.) at the bottom. This measurement may not, however, give a true indication of the imperfections in the specimen due to the presence of the local dents which are described in Section 3.3.

There seemed to be no correlation between the magnitude of the initial imperfections and the dimensions of the specimen. However, the maximum out-of-straightness was consistently observed in the two gage lines along either side of the weld.

3.1.3 Comparison with API Recommendations

The American Petroleum Institute recommends the following standards for allowable imperfections (13): 1) the difference between the maximum and minimum outside diameters should not exceed 1% of the nominal diameter (out-of-roundness) or 6.35 mm (¼ in.) for wall thickness less than 50 mm (2 in.), and 2) the out-of-straightness should not exceed 3.18 mm (1/8 in.) in any 3.05 m (10 ft) length.

Specimens T4, T5 and P11 exceeded the recommended standards for out-of-roundness. Specimen P11 exceeded the maximum difference between diameters requirement by 188% (11.9 mm, or 0.47 in.), and Specimen T5 exceeded the requirement by 22% (1.4 mm or 0.055 in.). These specimens also exceeded the out-of-roundness criterion by 19 to 32%. Specimen T4 exceeded the difference between diameters requirement by 84% (5.4 mm, or 0.21 in.) but met the out-of-roundness criterion. Based on a 3.05 m (10 ft) length, all of the specimens met the out-of-straightness criteria. These comparisons indicate that only Specimens T1, T2 and T3 were fabricated in accordance with current industrial practice.

3.2 Initial Shape

The initial shape of a specimen was determined with respect to an "ideal cylinder" which was visualized to have been superimposed over the specimen. The diameter of the ideal cylinder was computed as the average of the circumferences measured at each end of the specimen. The ends of the ideal cylinder were set to balance the inward and outward deviations of the specimen wall at the ends. This was approximately achieved by

making the ideal cylinder (actually, the ideal circle at the ends) pass through the two nearest grid points which straddled the largest diameter of the specimen. With the location of the ideal cylinder established, the offsets from this cylinder to the specimen wall were computed at each dial gage point along each gage line. These offsets are the initial deviations shown between the reference and the initial shape in Figs. 2, 3, 14, 15, and 37 to 42.

3.3 Local Imperfections

Some local imperfections were present in Specimens T3 and P11 that would not normally exist in fabricated tubular members. In Specimen T3 there were five areas of laminar separations which caused a local reduction of the wall thickness. Four of the areas were located near gage line 5 and one near gage line 8. All were more than 0.56 m (22 in.) from the top of the specimen (where local buckling occurred) and more than 1.0 m (40 in.) from the weld. The most severe area was located near gage line 8 and was approximately 38 mm long by 19 mm wide by 1.5 mm deep (1.5 in x 0.75 in. x 0.06 in.).

In Specimen P11 there were three dents which remained after the modification of the previously tested Specimen P9 to P11. The dents, as shown in Fig. 3, were located within 0.1 m (4 in.) of the top of the specimen and were directed radially inward up to 7.9 mm (0.31 in.) from a straight line along the wall of the specimen.

4. RESIDUAL STRESSES

4.1 General

The effect of residual stresses on the strength of steel structural members can be significant, and the magnitude and distribution of such stresses are greatly influenced by the method of fabrication and the geometry of the cross section. The objective of this investigation was to determine the influence of residual stresses on the pattern and the location of local buckles.

Circumferential stresses due to cold-rolling vary through the thickness of the plate, but as the stresses are essentially constant around a cross section they were not expected to affect the buckling pattern (14). Longitudinal stresses from the Poisson's ratio effect in cold-rolling and from the original cooling of the plate can be considered to be negligible in comparison to the welding residual stresses (15). As the longitudinal residual stresses due to welding were of major interest, these stresses were computed from measurements taken on Specimens T2 and T4.

4.2 Method of Measurement

The residual stresses were computed from the strain caused by the welding process. These strains were determined from the change in the distance between pairs of target holes which were located on the inside and outside surfaces of the specimen wall. The distances between the pairs of holes were measured with a Whittemore mechanical strain gage

with a 0.25 m (10 in.) gage length after the specimen had been rolled, but prior to welding the longitudinal seam, and then again after welding. As shown in Fig. 4, the holes were located 0.76 m (30 in.) from one end of the specimen to preclude the effect of the free end. The inside and outside pairs of holes were located opposite each other and were circumferentially spaced closer near the weld where the stresses were expected to change more rapidly. The holes were 1.2 mm in diameter by approximately 4 mm in depth (3/64 in.x 3/16 in.), and each had a countersunk shoulder on which to seat the tip of the measurement gage.

4.3 Discussion of Residual Stresses

The residual stress distributions computed in Specimens T2 and T4 are shown in Figs. 5 and 6. For the purpose of this presentation, the stress distribution around the circumference of the specimen is shown on a tube visualized to have been cut, unfolded, and laid out flat. The vertical line through the center corresponds to the weld seam, and the right and left edges correspond to the line which is diametrically opposite the weld on the specimen. The distance from the weld is given by the abscissa, and the stress is given by the ordinate. Computed stresses from both the inside and outside surfaces are plotted for a given distance from the weld, and the averages of these stresses are connected with a smooth curve.

At some locations there is a rather large difference between the inside and outside surface stresses. These differences may be attributed to longitudinal curvature or warping of the specimen wall, grinding of

the weld prior to re-rolling, holes not being located exactly opposite one another, disturbance of the targets, or damaged holes. Despite these differences, the smooth curve connecting the average of these readings does not vary significantly from the patterns determined in previous tests (5, 6, 16). The above reasons may also explain why the residual stress patterns presented are not fully symmetric about the weld, and why the stresses are not self-equilibrating.

The band of compressive stress extends from about 0.05 to 0.40 m (2 to 15 in.) on either side of the weld in Specimen T2 and has an average maximum stress of approximately 40 MPa (6 ksi). This zone in Specimen T4 extends from about 0.03 to 0.65 m (1 to 25 in.) from the weld and has an average maximum stress of approximately 60 MPa (9 ksi). The width of the residual compressive stress band increased with increasing specimen diameter. Beyond the compression zones the magnitude of the stress diminishes and tends to fluctuate between compression and tension in a wave-like pattern.

Specimens T2 and T4 can also be compared to three other tubular specimens fabricated from 350 MPa (50 ksi) steel whose welding residual stresses were measured previously. Specimen T2 was similar in geometry to Specimens P1 and P2 of Ref. 16. The width of the compressive bands was similar in all three tubes (approximately 0.45 m or 18 in.), but the maximum compressive stress in Specimen T2 was only about 65% of the stresses found for Specimens P1 and P2 (16). Specimen T4 was geometrically similar to Specimen P5 of Ref. 5. The compressive stress bands were

approximately 0.60 m (24 in.) in width, but the maximum stress in Specimen T4 was again only about 65% of the stress measured in Specimen P5 (5). Thus, it appears that the width of the compressive band is dependent on the geometry of the specimen, whereas the magnitude of the maximum stress is dependent on the yield stress.

5. TEST PROCEDURE

5.1 Test Setup

The general test setup for the specimens is shown schematically in Fig. 7. As illustrated in Fig. 25, the larger specimens stood in a five million pound hydraulic testing machine between the loading head and the machine floor. For convenience in taking measurements during the testing, Specimen T5 stood between the loading head and the machine pedestal, as illustrated in Fig. 31. The specimens were whitewashed with a lime solution in order to give a visual indication of the surface yielding during the test.

Alignment was accomplished by centering the specimen in the testing machine and by plumbing with a four foot level. To further assure the application of a uniform, concentric load to the specimen, a layer of gypsum ("Hydrostone") grout was placed between each of the end rings and the testing machine components. In order to form smooth contact surfaces, a small initial load (less than 2.5% of the predicted buckling load) was applied to the specimen before the grout could set.

5.2 Instrumentation

The instrumentation consisted of both mechanical dial gages and electric-resistance strain gages. Four mechanical dial gages at the corners of the machine head were used to measure the longitudinal shortening of the specimen. Two additional mechanical dial gages located diametrically opposite one another were attached between the end rings close to the wall

of Specimens T1 to T5. Three electric-resistance strain gages located at third points around the circumference and at approximately midheight of the specimen served as a check on the concentricity of the load and as an additional means for determining longitudinal deformations. For Specimens T2 and T4 these deformations were further checked with Whittemore strain gage readings which were taken periodically between the residual stress target holes.

The lateral deflection of the specimen wall relative to its ends was measured by means of the special movable dial gage rig shown standing at the side of the specimen in Figs. 25 and 31. The rig consisted of seven or eight mechanical dial gages attached to either an aluminum truss or an aluminum channel. The bottom of the rig sat on the end ring and touched the specimen wall, and an electromagnet held the top of the rig against the specimen. Readings were taken at nine to thirteen locations around the circumference by successively repositioning the rig.

5.3 Test Sequence

Following the alignment of the specimen, readings were taken of all gages to serve as the initial reference. Generally, load increments of 445 kN (100 kips) were slowly applied until the load reached approximately 85% of the expected buckling load. The load increments were then reduced to 220 kN (50 kips) as the buckling load was approached.

At all load levels prior to buckling, readings were taken of the longitudinal dial gages and the electric-resistance strain gages. At

several of the load levels, readings from the dial gage rig were also taken. In addition, on Specimens T2 and T4, Whittemore strain gage readings were periodically made. After buckling, only the longitudinal dial gages and the electric-resistance strain gages were read since the buckling prevented the use of the dial gage rig.

6. TEST RESULTS

6.1 General Specimen Behavior

6.1.1 Prebuckling Behavior

The behavior of a test specimen prior to buckling can be described by its stress-strain relationship. The stress-strain curves for Specimens T1 to T5, and P11 are shown in Figs. 8 to 13, respectively. The ordinate in these figures is the average axial stress nondimensionalized with respect to the static yield stress, and the abscissa is the strain. In this investigation the strain was obtained by several different methods. Two measures of strain obtained for all of the specimens were: 1) the average of the three electric-resistance strain gage readings, and 2) the average axial deformation measured by the four corner longitudinal dial gages divided by the overall specimen length. In Specimens T1 to T5 strain was also computed as the average axial deformation measured by the two near longitudinal dial gages divided by the overall specimen length. In addition, in Specimens T2 and T4, average strains were computed from Whittemore strain gage readings.

The strain curves computed from longitudinal deformations generally had an initial nonlinear region (due to self-adjustments in the grouted ends) up to about 0.1 F/F_{ys}. The deviation from linearity was greater in the curves computed from the corner deformations than in the curves

computed from deformations measured near the specimen wall. The strain curves based on electric-resistance and Whittemore readings were linear from the start and agreed almost identically with one another. All of the curves remained linear to a stress of approximately 0.7 F/F_{ys}. Specimens T1 and T5 became nonlinear near this stress and strained extensively with increasing stress prior to the formation of the buckles. Specimens T2 and T3 behaved linearly up to stresses of approximately 0.9 F/F_{ys} before becoming nonlinear. The behavior of Specimens T4 and P11 remained essentially linear up to the buckling stress.

Lateral deflections were measured in the specimens prior to the formation of the buckles. Typical profiles are shown in Figs. 14 and 15 for Specimens T3 and T5. The sketch to the left (not drawn to scale) shows the buckled specimen, and the three profiles are for the gage lines indicated. The profiles are the deflections from the ideal cylinder. The lower set of profiles for gage line 9 in Fig. 15 is based on deflections with respect to the initial shape measurements along the line. The small circled numbers indicate the sequence of the profile changes during the testing. The profile numbered 3 was measured just prior to buckling.

The changes in the lateral deflections in Specimen T3 are generally less than those in T5, which seems to be consistent with the appearance of the buckled specimen. However, the profiles do not seem to correspond to the initial shape of the specimen. This is apparent in Fig. 15 for

Specimen T5, for which the pattern of buckles in the left sketch has no correlation with the prebuckling profiles.

6.1.2 Behavior at Buckling

At stresses near buckling the elastic response of Specimens T1, T2, T3, and T5 became quite sensitive to the rate of loading. After a particular load level was reached and the machine stopped, and during the time when instrumentation readings were being taken, the load gradually dropped to a lower (static) level even though the rate of loading was very slow. When testing was resumed the load climbed above the previously reached level, but again fell when the machine was stopped. This behavior is shown in Fig. 22 by the dashed lines between the static and the dynamic (at a very slow rate of loading) load-deflection curves. Since the buckling and the ultimate stresses were reached during the application of a load increment in all of the specimens except T4, the maximum load reached is used in the description of the prebuckling and the buckling behavior although the corresponding "static" load would represent the specimen capacity more properly.

Local buckling occurred in all of the test specimens. The ultimate stress reached was limited by the formation of buckles in all of the specimens except T1 and T5. The stress in these two specimens continued to climb above the stress at which buckling was first observed. The nondimensional buckling stress of each specimen is listed in Column 11 of Tables 1 and 1A.

Specimens T1 to T5 buckled at one end through the gradual formation of a uniform, circumferential ring bulge approximately 0.10 to 0.15 m

(4 to 6 in.) in width. Surface yielding was quite extensive over the length of Specimens T1 and T5, but the yielding was localized in the buckled regions of the other specimens. Specimens T1 and T5 also showed a tendency of forming additional ring bulges (in a wave-like pattern) along the length of the specimen prior to buckling at the end. Typical ring bulges are illustrated in Figs. 27 and 33. Specimen P11 buckled suddenly with an explosive sound into a diamond-shaped pattern, as shown in Fig. 35.

6.1.3 Post-Buckling Behavior

Buckling was followed by a sudden reduction in the applied stress in Specimens T2, T3, T4, and P11. Specimens T1 and T5 continued to carry significant additional stresses after buckling had been visibly detected. After local buckling occurred, most of the increase in deformation was concentrated in the buckled regions. The strains from the electric-resistance gages and the average strains did not accurately represent the behavior of the buckled portion of the specimen. A more valid representation of the overall specimen behavior in the post-buckling range is the stress-deformation relationship. These curves are shown for each specimen in Figs. 16 to 21. In these figures the ordinate is the nondimensional stress and the abscissa is the average longitudinal deformation measured by the four corner dial gages.

The postbuckling capacities of the specimens stabilized at 12 to 23 percent of the buckling strength at an overall longitudinal shortening of 75 to 150 mm (3 to 6 in.). As shown in Figs. 28 and 34, further

longitudinal compression resulted in the transformation of the ring bulge into a polygonal shape. The orientation of the polygon with respect to the weld was random, but the number of sides increased with an increasing D/t.

Additional compression always resulted in the specimen wall folding over onto itself, and after the folds contacted either the specimen wall or an end ring, slightly increased loads could be carried until a second layer of buckles formed. These increases in stress are indicated by the rising portions of the curves in the post-buckled regions of Figs. 16, 17, 19 and 20.

6.2 Behavior of Individual Specimens

6.2.1 Behavior of Specimen T1

The stress-strain curves for Specimen T1 are shown in Fig. 8. The strains computed from longitudinal deformations measured near the specimen wall were nearly the same as those read from the electric-resistance gages, and these strains were approximately 0.0003 less than the strains obtained from the corner longitudinal deformations. The curves began to deviate from linearity at approximately 0.7 F/F_{ys}. At a stress of 0.85 F/F_{ys}, surface yielding became apparent as the whitewash began flaking off the specimen along both sides of the weld over the full length of the specimen (regions of maximum residual compressive stress). Yielding soon spread completely around the specimen at midheight, and later progressed to form 14 to 16 equally spaced circumferential rings, as shown in Fig. 24. The specimen seemed to be on the verge of

forming a series of ring bulges (which would have given the specimen a corrugated appearance), but the lateral deflections did not develop over the length. Small ring bulges did initially appear at both ends of the specimen. Upon reaching the ultimate stress of 1.07 F/F_{ys} the deformation became concentrated in the bottom ring, and the top ring relaxed into a nearly straight position.

As the compression was continued beyond the maximum load, the bottom ring bulge was transformed into a three-sided polygon. As shown in Fig. 16, the post-buckling capacity stabilized at approximately 0.23 F/F_{ys}, and the capacity increased to approximately 0.50 F/F_{ys} prior to the formation of the second set of buckles. The second set was also three-sided, but it was offset by a half wave just above the first pattern.

6.2.2 Behavior of Specimen T2

The stress-strain behavior of Specimen T2 is shown in Fig. 9. The strains computed from the longitudinal deformations measured near the specimen were approximately midway between the strains read from the strain gages and the strains computed from the corner longitudinal deformations. At a stress of approximately 0.90 F/F_{ys} the curves became nonlinear and surface yielding was observed along both sides of the weld near the top of the specimen. At the ultimate stress of 1.00 F/F_{ys}, the uniform ring bulge illustrated in Figs. 26 and 27 appeared at the top. These photographs also show that surface yielding occurred

only in the buckled portion of the specimen. Fig. 17 shows the decrease in the applied stress that immediately followed buckling. After additional compression, the ring bulge was transformed into a three-sided pattern, and a stable post-buckling capacity of 0.18 F/F_{ys} occurred at approximately 90 mm (3.5 in.). Prior to the formation of the second set of buckles illustrated in Fig. 28, a maximum postbuckling stress of 0.37 F/F_{ys} was reached.

6.2.3 Behavior of Specimen T3

Fig. 10 shows the stress-strain curves for Specimen T3. The strains computed from the longitudinal deformations measured near the specimen were very similar to those read from the electric-resistance strain gages. In the linear portion of the curves these strains were approximately 0.0002 less than the strains computed from the longitudinal deformations measured at the corners of the loading head.

Specimen T3 was loaded to a stress of 0.80 F/F_{ys} during the first day of testing and then unloaded to 0.40 F/F_{ys} before leaving it overnight. When testing was resumed the previous loading path was retraced, and a stress of approximately 0.90 F/F_{ys} was reached before the behavior became nonlinear. Yielding was first observed at the top of the specimen in a very narrow band along the weld toe of the end ring at a stress of 0.97 F/F_{ys}. At a stress of 1.00 F/F_{ys} a ring bulge began to form at the top. Two additional load increments were applied before the ring bulge extended completely around the specimen. Fig. 18 shows that

immediately after buckling the applied stress dropped to approximately 0.50 F/F_{ys} and later stabilized in the post-buckling region at 0.18 F/F_{ys}. The ring bulge developed into a four-sided polygon during this post-buckling deformation. The final view is shown in Fig. 29.

6.2.4 Behavior of Specimen T4

The stress-strain behavior of Specimen T4 is shown in Fig. 11. The strains computed from longitudinal deformations measured near the specimen wall were approximately midway between the strains read from the electric-resistance gages and those computed from the corner longitudinal deformations.

At a stress of 0.47 F/F_{ys} some local yielding was observed at the top of the specimen along the weld toe of the end ring. The yielding did not spread significantly until stresses were near the ultimate, and the stress-strain and load-deformation curves remained linear. During the first day of testing a stress of 0.54 F/F_{ys} was reached, but the specimen was unloaded to 0.37 F/F_{ys} before leaving it overnight.

When testing was resumed the following day, these same linear paths were followed. The behavior remained essentially linear up to the ultimate stress of 0.88 F/F_{ys}. The ultimate stress was reached under essentially static conditions, as no loading was being applied and instrumentation readings were being taken when buckling occurred. The ring bulge formed rather suddenly and was followed by the large drop in the applied stress level shown in Fig. 19. The post-buckling stress

stabilized at approximately 0.13 F/F_{ys}.

With additional deformation the ring bulge eventually transformed into a six-sided polygon. Testing continued until a second set of buckles formed. As the specimen wall folded over, as shown in Fig.30, cracks appeared right under the folds.

6.2.5 Behavior of Specimen T5

The stress-strain curves for Specimen T5 are shown in Fig. 12. The strains computed from longitudinal deformations near the specimen wall were essentially the same as the strains read from the electric-resistance gages. For a given increase in stress, these strains increased at a slightly slower rate than the corresponding strains computed from the corner longitudinal deformations. The difference between the strains varied from about 0.0005 to 0.0008.

Surface yielding was first observed near the weld at a stress of 0.94 F/F_{ys}. Two yield lines formed at 0.20 and 0.38 m (8 and 15 in.) from the top of the specimen and a third yield line later appeared between the two. At a stress of 1.07 F/F_{ys} surface yielding became concentrated near the bottom of the specimen, and a wave-like pattern of four buckles formed along the length. The shadow cast on the right side of the specimen in Fig. 32 shows the wave-like pattern, which was most pronounced near the weld. At a stress near 1.11 F/F_{ys} the bottom wave grew into the ring bulge shown in Fig. 33, and the level of stress dropped as shown in Fig. 20. The stress level stabilized at 0.25 F/F_{ys}, and a three-sided polygon pattern developed from the ring bulge.

As the wall of the specimen deformed as shown in Fig. 34, the weld cracked at the fold. The wave-like rings retained most of their initial magnitudes during the post-buckling deformation.

6.2.6 Behavior of Specimen P11

Figure 13 shows the stress-strain behavior of Specimen P11. During the first day of testing a stress of 0.80 F/F_{ys} (87% of the buckling stress of Specimen P9) was reached, then the specimen was unloaded to 0.26 F/F_{ys} before leaving it overnight. When testing was resumed, the stress-strain curve computed from longitudinal deformations was parallel, but offset, from the previous curve, thus indicating the presence of some plastic deformations. Strains read from the electric-resistance gages were also slightly offset, but the differences were negligible for the scale used in the figure. For a given increase in stress, the strains computed from the corner longitudinal deformations increased at a slightly greater rate than the corresponding strains read from the electric-resistance gages. The curves deviate only slightly from linearity just prior to reaching the buckling stress.

Buckling occurred with an explosive bang at an ultimate stress of 0.83 F/F_{ys}. Initially, three diamond-shaped buckles formed near the top of the specimen, two on one side of the weld and one on the other. Without further loading, seven additional buckles formed and the resulting pattern shown in Fig. 35 circled the specimen.

As shown in Fig. 21, the applied stress dropped suddenly after buckling, and the post-buckling strength stabilized at a stress of

0.10 F/F_{ys}. During additional compression, the wall of the specimen folded over as shown in Fig. 36, and cracks appeared under the folds.

7. DISCUSSION OF TEST RESULTS

7.1 General Specimen Behavior

7.1.1 Prebuckling Behavior

The stress-strain curves for T1 to T4 in Figs. 8 to 11 show a considerable difference among the strains measured at a particular stress. The larger initial strains computed from the corner dial gage readings may be attributed to the compression of the capping grout on the specimens and other initial adjustments that would affect the overall deformation of the specimen but would not be reflected in the local strains measured by the electric-resistance gages. After the initial nonlinearities, the slopes of the stress-strain curves are very similar and compare favorably with the assumed modulus of elasticity of 203,400 MPa (29,500 ksi).

This consistency among the stress-strain slopes of the A36 specimens was not observed in Specimen P11 with the yield stress of 700 MPa (100 ksi) or in the previous tests conducted on high-strength steel specimens (16). It was assumed that the difference in slopes may have been caused by the deflection of the corners of the testing machine loading platen. To check this assumption, Specimens T1 to T5 had two dial gages located near the specimen

wall to measure the longitudinal deformations. The strains computed from these two near gages would then be expected to approach the strains read from the electric-resistance gages since the effects of platen bending in the machine would be eliminated. This theory does not appear completely valid, however, since the slopes of the stress-strain curves for Specimens T1 to T4 were very similar.

There is one additional inconsistency that exists in the magnitude of the strains computed from the two near dial gages. Figures 9 and 11 (Specimens T2 and T4) indicate, as expected, that these strains are between the strains read from the electric-resistance gages and those computed from the corner longitudinal deformations. However, Figs. 8,10, and 12 (Specimens T1, T3, and T5) show that the strains computed by the two near gages were nearly the same as those read from the electric-resistance gages. No explanation other than the particular conditions of the individual tests can be made for these discrepancies.

The lateral deflection profiles shown in Figs. 14 and 15 must be viewed with some caution. When measurements were being taken with the dial gage rig it was assumed that the ends of the rig were positioned at a fixed location on a straight line relative to the ends of the specimen. However, in some specimens the magnet holding the rig against the specimen wall was near the location where the ring bulges appeared. Consequently, any lateral deflections in this region would have affected the dial gage readings. It was also observed that the

variation among readings which were taken against the flat reference surface may have exceeded the magnitude of the actual deflection in the specimen for a given load increment.

7.1.2 Behavior at Buckling

In most specimens buckling occurred at one end. A possible explanation for this is that due to Poisson's ratio the wall of the specimen desires to expand laterally as the specimen is compressed. The ends of the specimen are restrained from expansion by the end rings, thus inducing local bending moments which act in combination with the axial load. In previous research where end rings were not added, buckling still commonly occurred at the ends (5). In these cases the restraint was probably offered by the friction between the ends of the specimen and the testing machine. This preferential location for buckling was not so obvious in Specimens T1 and T5, as both showed a tendency to form ring bulges at other locations along the length.

The buckling stress was not clearly defined in the specimens with low D/t ratios and high straining capacities. Ring bulges were observed in Specimens T1 and T5 at stresses below the ultimate. For such specimens the use of a critical strain may perhaps be a more meaningful parameter to define the point of buckling.

7.1.3 Post-Buckling Behavior

The post-buckling stress of the specimens stabilized within a range of 12 to 23 percent of the buckling stress. This range is similar to that previously observed for high-strength specimens (4,16). Some additional stresses could be carried after the wall of the specimen had folded over and come into contact with the unbuckled wall or an end ring. It appears that the points of contact provided the additional longitudinal support required for the formation of the second set of buckles.

7.2 Comparison of Specimen Behavior

7.2.1 Comparison of Specimens T1 and T5

Specimens T1 and T5 had D/t ratios less than 80, L/r ratios less than 8, and a nominal thickness of 9.5 mm (3/8 in.). Figures 8 and 12 show that the specimens had the capacity to strain quite extensively prior to buckling. The extensive surface yielding which occurred prior to buckling is illustrated in Figs. 24 and 32. Each specimen was able to carry a stress above the stress at which the formation of buckles became visible. Each specimen showed a tendency to form a series of longitudinal waves (or circumferential ring bulges) along its length with the larger initial rings near the ends. The final ring bulge formed near the bottom of the specimen, and it transformed into a three-sided polygonal pattern during the post-buckling deformation. Figure 23 shows that the stress-deformation behavior was nearly identical up to a stress of 1.00 F/F_{ys}, and also that the post-

buckling behavior was similar. The post-buckling stress stabilized at approximately 0.24 F/F_{ys} at a deformation of approximately 0.12-0.13 m (5 in.).

7.2.2 Comparison of Specimens T2, T3, and T4

Specimens T2, T3, and T4 were fabricated from the same plate but had D/t ratios from 113 to 226 and L/r ratios from 5.6 to 8.5. Figures 9 to 11 and 17 to 19 indicate that the specimens deviated very little from linear behavior prior to buckling. The buckling strain was approximately 0.001 to 0.002, and the deformation at buckling was approximately 6 mm (0.24 in.). The buckling stresses were near 1.00 F/F_{ys} for Specimens T2 and T3 and 0.88 F/F_{ys} for T4. The stable post-buckling stress level for Specimen T4 was about 20% less than that of T2 or T3. Formation of the ring bulge occurred near the top of each specimen with relatively little prior surface yielding.

The premature local yielding which was observed in Specimen T4 and the comparatively lower ultimate stress may lead to some suspicions concerning the magnitude of the buckling stress. The local yielding described in Section 6.2.4 was probably caused by the concentrated stresses that could have resulted from insufficient grout covering over some metal projections on the top end ring of the specimen. However, a similar pattern of local yielding was observed in Specimen T3 (but at a higher level of stress), which had no metal projections. The fact that linearity in the stress-strain and the stress-deformation curves (Figs. 11 and 19) was not disturbed and that the

stable post-buckling stress was also lower than the corresponding stresses in T2 and T3 lend credibility to the buckling stress results.

7.2.3 Comparison of Specimens P11 and P9

Specimen P11 was made by modifying the previously tested Specimen P9 (7). As shown in Fig. 21, Specimen P11 followed nearly the same linear stress-deformation path as P9 but buckled at a stress of 0.83 F/F_{ys} compared to 0.91 F/F_{ys} for P9. Two previous retests showed that the buckling stress should be nearly the same in both the original and the modified specimens (Specimens P3 and P3A of Ref. 5 and P6 and P8 of Refs. 6 and 7). This indicates an apparent effect of the relatively large geometric imperfections, which are described in Chapter 3 and Section 7.3, on the buckling stress. The level of the stable post-buckling stress was 0.08 to 0.10 F/F_{ys} for the specimens.

7.3 Effect of Initial Imperfections

There seemed to be no correlation in the A36 specimens between the initial imperfections and the buckling pattern or location, as each of these specimens failed initially through the formation of a ring bulge. Column 8 of Tables 3 and 3A lists the type and the location of the initial local buckling in each specimen. Figures 37 to 41 show the polygonal post-buckling patterns of Specimens T1 to T5 superimposed on the initial shape. The buckled shape, shown by the dark solid line in the figures, does not represent a particular stress level nor is it drawn to a specific scale. A comparison among the

figures indicates that no correlation exists between the orientation of the polygon post-buckling pattern and the initial deflections.

The initial indentations and the buckling pattern of Specimen P11 are shown in Fig. 42. Two of the initial dents are near the locations where the specimen buckled inward, but the third dent was located where the specimen buckled outward. The reduction in the buckling stress of Specimen P11 compared to that of P9 seems to indicate that imperfections with magnitudes that approach the thickness of the specimen wall, and with patterns similar to the potential buckling pattern, may have some effect on the level of the buckling stress.

During testing, no local yielding or other disturbances were observed near the laminations in Specimen T3. The laminations seemed to have no effect on either the buckling stress or the buckle pattern.

7.4 Effect of Residual Stresses

Figures 5 and 6 indicate that a narrow band of high tensile residual stress exists at the longitudinal weld. This is confirmed by Fig. 24, which shows a lack of surface yielding (light areas on the photograph) along the weld in an otherwise extensively yielded specimen. Figures 5 and 6 also indicate the regions and magnitude of maximum compressive residual stress, and these were generally the first to show signs of surface yielding. However, each of the A36 specimens (T1 to T5) failed initially through the formation of a uniform, circumferential ring bulge at one end, and as shown in Figs. 37 and 41, the polygonal post-buckling pattern that later developed was randomly

oriented. Thus, it appears that the welding residual stresses had no effect on the buckling pattern of the tubular specimens. This confirms the conclusion that was reached previously for the effect of residual stresses on high-strength steel tubular specimens (5,16).

7.5 Effect of D/t Ratio

The nondimensional buckling stress of each specimen and the D/t ratio are listed in Tables 1 and 1A and plotted in Fig. 43. Also shown in the figure are some of the results from previous tests conducted on fabricated tubular columns (5,6,7,9).

The buckling stresses generally decreased with increasing D/t ratios. At D/t ratios less than 100 the buckling stress was nearly equal to or exceeded the static yield stress. The occurence of buckling stresses above yield was probably caused by strain-hardening due to cold working of the rolling process and/or by the strain rate at the time of loading as indicated in Fig. 22 for Specimen T5.

7.6 Effect of α and c

Nondimensional parameters α and c are used in the presentation of test data. They tend to reduce the scatter among the test results for specimens with different yield stresses. The parameter α is defined by

$$\alpha = \frac{E}{F_y} \cdot \frac{1}{D/t} \qquad (2)$$

The buckling stress and α for each specimen are given in Tables 1

and 1A and plotted in Fig. 45. Also shown are some of the results from previous tests conducted on fabricated tubular columns (5,6,7,9).

Previous research conducted on high-strength steel specimens reported a trend for the mode of buckling to be dependent on α (16). The A36 specimens followed this trend, that is, for α greater than 2.4 buckling occurred gradually through the formation of a uniform ring bulge. There were no A36 specimens tested with α less than 2.4. Specimen P11, with α less than 2, also followed this guideline by failing suddenly through the formation of a series of diamond-shaped buckles.

Parameter c was used in Ref. 4 to propose an equation for predicting the local buckling strength of 350 MPa (50 ksi) steel tubular columns. Parameter c is defined by

$$c = \sqrt[3]{\frac{E}{F_y}} \cdot \frac{1}{D/t} \qquad (3)$$

The buckling stress and c for each specimen are given in Tables 1 and 1A and plotted in Fig. 46. The use of c reduced the scatter among test results much more effectively than the use of α.

In computing α and c for Table 1 and for Figs. 45 and 46, the static yield stress F_{ys} was used for the yield stress F_y of Eqs. 2 and 3. When the test data did not indicate how the yield stress was determined, such as in Reference 9, the yield stress was assumed to be dynamic and it was used without any adjustments for F_y.

7.7 Comparison of Test Results with Design Curves

Several local buckling design curves which are in current use (1,17,18) are shown in Fig. 45 together with test results on fabricated cylindrical columns. The nondimensional parameter α is used as the abscissa. The optimistic DNV curve gives the best correlation with the test results except for Specimen T4, whose buckling stress falls about 7% below the curve. All of the other design curves are conservative in comparison with the test results.

The following design curve, proposed by the API Mini-Committee on tubular columns (19), has been approved for inclusion in the 11th edition (1980) of the API specification RP 2A (20):

for $D/t \leq 60$

$$\frac{F_c}{F_y} = 1.00 \tag{4a}$$

for $60 < D/t < 300$

$$\frac{F_c}{F_y} = 1.64 - 0.23\sqrt[4]{D/t} \tag{4b}$$

As can be seen in Fig. 43, this curve is quite conservative when the static yield stress F_{ys} is used as the non-dimensionalizing value for the yield stress F_y.

However, the prudent intent of the API Mini-Committee developing Eq. 4 from the test data was to be on the conservative side by using the ASTM dynamic yield stress F_{yd} which is the industry acceptance standard. In this case, as shown in Fig. 44, Eq. 4 becomes a reasonable and conservative approximation of the test results. In Fig. 45, Eq. 4 is plotted for comparison with other curves. It is more conservative for lower D/t and less conservative for higher D/t than the old API rule (17).

One of the objectives of the work presented here was to check whether the local buckling equation proposed in Reference 4 for tubular members made from 350 MPa (50 ksi) steel would also be applicable to members made from 250 MPa (36 ksi) steel. A slightly modified version of that equation is

for $c < 0.07$

$$\frac{F_c}{F_y} = 38\ c - 480\ c^2 + 2020\ c^3 \qquad (5)$$

for $c \geq 0.07$

$$\frac{F_c}{F_y} = 1.0$$

where c is defined by Eq. 3.

Figure 46 shows the curve corresponding to Eq. 5 and the test results nondimensionalized with respect to the static yield stress F_{ys}. The curve correlates with the test results very closely and is somewhat conservative with respect to the three points on the left side which are the test results on specimens with static yield stress F_{ys} = 350 MPa (50 ksi) and greater.

Thus, it can be concluded that Eq. 5 gives an accurate prediction of the local buckling stress of cylindrical tubular columns made from steels with static yield stress F_{ys} of 250 MPa (36 ksi) and it may be conservative for higher values of F_{ys}. In the application of this equation to practical design, careful consideration should be given

to the significance of the difference between the static F_{ys} and dynamic F_{yd} yield stresses.

8. SUMMARY AND CONCLUSIONS

Local buckling tests were conducted on six tubular specimens fabricated by cold-rolling flat plate into a cylindrical shape and then welding the joint. Five of the specimens were made from 250 MPa (36 ksi) steel, and one by modifying a 700 MPa (100 ksi) specimen tested previously. The outside diameters ranged from 0.58 m (23.02 in) to 1.53 m (60.30 in) and the thicknesses from 6.73 mm (0.265 in) to 9.94 mm (0.391 in). The corresponding diameter-to-thickness ratios (D/t) ranged from 59 to 233. The slenderness ratios (length-to-radius of gyration) were less than 9 to preclude the effect of overall column buckling.

Local buckling occurred in each of the specimens. The ultimate stress reached was limited by buckling in four of the specimens, but in two a slight increase in stress was achieved after buckling could be visibly detected. The influence of initial geometric imperfections and welding residual stresses on the location and pattern of the buckles was examined, as well as the behavior of the specimens in the post-buckling region. The test results were examined using several design parameters and equations.

The following conclusions can be drawn from the results of these tests:

1) The design rules for local buckling which are currently recommended by the API and AISI are adequately conservative for tubular members fabricated from 250 MPa (36 ksi) steel which fall within the range of parameters tested ($59 \leq D/t \leq 227$ and $4.41 \leq \alpha \leq 11.09$).

2) The nondimensional buckling stresses for the 250 MPa (36 ksi) specimens are in good agreement with the 350 MPa (50 ksi) specimens tested previously when nondimensionalized with respect to F_{ys} and plotted versus parameter c.

3) The test results from the 250 MPa (36 ksi) specimens are not as consistent as those from the 350 MPa (50 ksi) specimens. This may be attributed to the higher sensitivity of the 250 MPa steel to the strain rate during testing.

4) The post-buckling strength depends on D/t (or α, or c). In general, the post-buckling strength will decrease with an increase in D/t.

5) By forming successive sets of buckles, tubular columns can effectively dissipate energy at approximately 12-23% of the buckling stress.

6) There is no apparent correlation between the pattern of longitudinal residual stresses due to welding and the pattern of local buckling.

7) The width of the compressive residual stress band on each side of the weld appears to be dependent on the diameter of the specimen, whereas the magnitude of the maximum compressive stress seems to be dependent on the yield stress level.

8) Initial geometric imperfections whose magnitudes are of the order of those established by the API specifications appear to have no apparent influence on either the local buckling stress or the pattern of the buckles for the range of parameters tested.

9) Imperfections of the order of magnitude of the plate thickness and distributed in a manner similar to the buckling pattern appeared to adversely influence the buckling stress in one specimen (Specimen P11).

10) The mode of initial buckling conformed to the previously established guidelines which were based on the value of α. For specimens with α greater than 3.6 (Specimens T1 to T5), the mode was a gradual formation of ring bulge, and for specimens with α less than 2.4 (Specimen P11), it was sudden buckling into a diamond-shaped pattern.

9. RECOMMENDATIONS

Since Eq. 5 gives a more accurate prediction of the local buckling stress for cylindrical tubular columns fabricated from steel with a static yield stress level F_{ys} from 250 MPa (36 ksi) to 700 MPa (100 ksi) than other available methods, this equation is recommended as a basis for developing design criteria. In this, attention should be paid to the statistic significance of the difference between the static and dynamic yield stresses.

As research conducted so far on the local buckling of fabricated tubular columns has covered only relatively stocky members ($D/t < 227$ for $F_{ys} = 250$ MPa and $D/t < 295$ for $F_{ys} = 350$ MPa), it is recommended that additional tests be conducted on specimens with larger D/t ratios, so that Eq. 5 could be verified for such D/t ratios and/or a more comprehensive new formulation developed.

At present only approximate consideration is made of local buckling in the design of long tubular columns which are subject to interaction between local and overall buckling (4). It is therefore recommended that a research program be initiated on the effect of local buckling upon the overall buckling strength of long cylindrical columns.

10. ACKNOWLEDGMENTS

This investigation was conducted at the Fritz Engineering Laboratory, Lehigh University. Dr. Lynn S. Beedle is Director of the Laboratory and Dr. David A. VanHorn is Chairman of the Civil Engineering Department. The research was sponsored by the American Petroleum Institute as PRAC Project No. 16 guided by the Technical Advisory Committee which consisted of the following

R. K. Kinra (Dr.) - Chairman	R. M. Meith
C. Capanoglu	C. D. Miller
J. W. Cox (Dr.)	D. R. Sherman (Prof.)
R. R. Graham, Jr.	J. A. Tegtmeier

The authors are grateful for the competent professional guidance and advice given by this committee.

Sincere thanks are expressed to Dr. Roger G. Slutter and the technical staff of the laboratory, especially Messrs. Robert Dales, Kermit Eberts, Charles Hittinger, and Russell Logenbach, for their assistance in setting up and conducting the tests. Special thanks are due to Messrs. Michael Salley and Andre Vaucher for their assistance during the tests, in the reduction of the experimental data, and the production of the report. Gratitude is also expressed to Ms. Karen Daley for her careful and patient typing of the report.

11. NOMENCLATURE

A = cross-sectional area

c = nondimensional parameter = $\sqrt[3]{\frac{E}{F_y}} \cdot \frac{1}{D/t}$

D = mean diameter = OD-t

E = modulus of elasticity = 203, 400 MPa (29,500 ksi)

F = nominal axial stress = $\frac{P}{A}$

F_c = local buckling stress

F_y = yield stress (nominal, static, or dynamic as applicable)

F_{ys} = static yield stress

F_{yd} = dynamic yield stress

L = length

L/r = slenderness ratio

P = axial load

r = radius of gyration = $\sqrt{\frac{I}{A}}$

t = thickness

α = nondimensional parameter = $\frac{E}{F_y} \cdot \frac{1}{D/t}$

12. REFERENCES

1. Johnston, B. G., Editor
   GUIDE TO STABILITY DESIGN CRITERIA FOR METAL STRUCTURES, Chapter 10, Structural Stability Research Council, 3rd ed., John Wiley and Sons, Inc., New York, N.Y., 1976.

2. Schilling, C. G.
   BUCKLING STRENGTH OF CIRCULAR TUBES, Journal of the Structural Division, ASCE, Vol. 91, No. ST5, p. 325, (October 1965).

3. Miller, C. D.
   BUCKLING OF AXIALLY COMPRESSED CYLINDERS, Journal of the Structural Division, ASCE, Vol. 103, No. ST3, p. 695, (March 1977).

4. Ostapenko, A.
   LOCAL BUCKLING OF WELDED TUBULAR COLUMNS, Proceedings of the International Colloquium on Stability of Structures under Static and Dynamic Loads (Washington, D.C., May 1977), ASCE, New York, p. 367, 1977.

5. Ostapenko, A. and Gunzelman, S. X.
   LOCAL BUCKLING OF TUBULAR STEEL COLUMNS, Proceedings, Methods of Structural Analysis, Vol. II, ASCE, New York, N.Y., p. 549, 1976.

6. Ostapenko, A. and Gunzelman, S. X.
   LOCAL BUCKLING TESTS ON THREE STEEL LARGE-DIAMETER TUBULAR COLUMNS, Proceedings of the Fourth International Conference on Cold-Formed Steel Structures, St. Louis, Missouri, p. 409, (June 1978).

7. Marzullo, M. A. and Ostapenko, A.
   TESTS ON TWO HIGH-STRENGTH STEEL LARGE-DIAMETER TUBULAR COLUMNS, Paper 3086, Proceedings of the 10th Offshore Technology Conference, Houston, Texas, (May 1978).

8. American Society for Testing and Materials
   1974 ANNUAL BOOK OF ASTM STANDARDS, PART 4, Specification A36-74, American Society of Testing and Materials, Philadelphia, Pennsylvania, 1974.

9. Wilson, W. M. and Newmark, N. M.
   THE STRENGTH OF THIN CYLINDRICAL SHELLS AS COLUMNS, Bulletin No. 255, Engineering Experiment Station, University of Illinois, (February 1933).

10. Wilson, W. M.
TESTS OF STEEL COLUMNS, THIN CYLINDRICAL SHELLS, LACED COLUMNS, ANGLES, Bulletin No. 292, Engineering Experiment Station, University of Illinois, (April 1937).

11. American Society for Testing and Materials
1971 ANNUAL BOOK OF ASTM STANDARDS, PART 31, ASTM Specification E8-69, American Society for Testing and Materials, Philadelphia, Pennsylvania, 1971.

12. Rao, N. R., Lohrman, M., and Tall, L.
EFFECT OF STRAIN RATE ON THE YIELD STRESS OF STRUCTURAL STEELS, Journal of Materials, Vol. 1, No. 1, P. 241, (March 1966).

13. American Petroleum Institute, Division of Production
API SPECIFICATION 2B, SPECIFICATION FOR FABRICATED STRUCTURAL STEEL PIPE, 3rd ed., Dallas, Texas, (1977).

14. Chen, W. F. and Ross, D. A.
TESTS OF FABRICATED TUBULAR COLUMNS, Journal of the Structural Division, ASCE, Vol. 103, No. ST3, p. 619, (March 1977).

15. Rao, N. R. and Tall, L.
RESIDUAL STRESSES IN WELDED PLATES, Fritz Laboratory Report 249.7, Lehigh University, Bethlehem, Pennsylvania (October 1960).

16. Gunzelman, S. X.
EXPERIMENTAL LOCAL BUCKLING OF FABRICATED HIGH-STRENGTH STEEL TUBULAR COLUMNS, Master's Degree Thesis, Fritz Laboratory Report 406.8T, Lehigh University, Bethlehem, Pennsylvania (October 1976).

17. American Petroleum Institute, Production Department
API RP 2A, RECOMMENDED PRACTICE FOR PLANNING, DESIGNING, AND CONSTRUCTING FIXED OFFSHORE PLATFORMS, 10th ed., Dallas, Texas, p. 21, (March 1979).

18. Det Norske Veritas
TENTATIVE RULES FOR DESIGN, CONSTRUCTION, AND INSPECTION OF FIXED OFFSHORE STRUCTURES, Rule Proposal RNT-1-73, (October 1973).

19. API PRAC Project No. 16
Committee Correspondence from R.K. Kinra to J.L. Hubbard dated August 23, 1979.

20. American Petroleum Institute, Production Department
API RP 2A, RECOMMENDED PRACTICE FOR PLANNING, DESIGNING, AND CONSTRUCTING FIXED OFFSHORE PLATFORMS, 11th ed., Dallas, Texas (to be published in 1980).

TABLE 1. SPECIMEN DATA

No.	Steel	Coupon Static F_{ys} (MPa)	Measured OD (m)	Measured t (mm)	Measured L (m)	$\frac{D}{t}$	$\frac{L}{r}$	α	c	Test $\frac{F_c}{F_{ys}}$
1	2	3	4	5	6	7	8	9	10	11
T1	A36	239.0	0.77	9.94	2.03	76.7	7.54	11.09	0.124	1.056
T2	A36	203.8	0.78	6.73	2.03	113.3	7.53	8.81	0.088	1.004
T3	A36	203.8	1.02	6.73	3.05	150.7	8.50	6.62	0.066	0.999
T4	A36	203.8	1.53	6.73	3.05	226.5	5.65	4.41	0.044	0.880
T5	A36	335.6	0.58	9.73	1.22	59.1	5.99	10.20	0.143	1.069 (1.009) *
P11	A514 Tp B	622.8	1.53	6.55	1.96	232.9	3.63	1.40	0.030	0.829

Notes:

$$\alpha = \frac{E}{F_y} \cdot \frac{1}{D/t}$$

$$c = \sqrt[3]{\frac{E}{F_{ys}}} \cdot \frac{1}{D/t}$$

*Static Value (See Fig. 22)

TABLE 1A. SPECIMEN DATA

No.	Steel	Coupon Static F_{ys} (ksi)	Measured OD (in.)	Measured t (in.)	Measured L (in.)	$\frac{D}{t}$	$\frac{L}{r}$	α	c	Test $\frac{F_c}{F_{ys}}$
1	2	3	4	5	6	7	8	9	10	11
T1	A36	34.67	30.40	0.391	80	76.7	7.54	11.09	0.124	1.056
T2	A36	29.56	30.30	0.265	80	113.3	7.53	8.81	0.088	1.004
T3	A36	29.56	40.21	0.265	120	150.7	8.50	6.62	0.066	0.999
T4	A36	29.56	60.30	0.265	120	226.5	5.65	4.41	0.044	0.880
T5	A36	48.67	23.02	0.383	48	59.1	5.99	10.20	0.143	1.069 (1.009)*
P11	A514 Tp B	90.32	60.29	0.258	77	232.9	3.63	1.40	0.030	0.829

Notes:

$$\alpha = \frac{E}{F_y} \cdot \frac{1}{D/t}$$

$$c = \sqrt[3]{\frac{E}{F_{ys}}} \cdot \frac{1}{D/t}$$

*Static Value (See Fig. 22)

TABLE 2 . TENSILE COUPON RESULTS

Source*	Coupon No.	Thick-ness (mm)	Yield Stress (MPa) F_{ys}	F_{yd} 52μm/m/sec	$\frac{F_{yd}}{F_{ys}}$	F_{yd} 1042 μm/m/sec	$\frac{F_{yd}}{F_{ys}}$	F_u (MPa)
1	2	3	4	5	6	7	8	9
Specimens T2, T3, and T4: nominal 6.4 mm plate								
1						262.0+		
2	T22	6.78	203.3	222.4	1.09			367.2
	T23	6.79	206.8	222.9	1.08			368.6
	T24	6.79	202.4	218.4	1.08			369.5
3	L7	6.68	204.1	226.2	1.11	239.3	1.17	
	L8	6.65	203.4	224.8	1.10	239.9	1.18	
	L9	6.69	202.7	225.5	1.11	237.9	1.17	
4	L2					264.1+		
	L3					257.9+		
	L4					279.2+		
	Average	6.73	203.8	223.4	1.10	239.0	1.17	368.4
Specimen T1: nominal 9.5 mm plate								
1						268.2		
2	T11	9.87	242.7	255.7	1.05			424.5
	T12	9.90	246.6	270.1	1.09			420.0
	T14	9.90	244.3	265.5	1.09			422.5
3	T15	9.98	231.7	251.0	1.08	259.9	1.12	
	T19	9.99	235.1	257.2	1.09	271.0	1.15	
	T20	9.99	233.7	255.1	1.09	265.5	1.14	
	Average	9.94	239.0	259.1	1.08	265.5	1.14	422.3
Specimen T5: nominal 9.5 mm plate								
5						363.4		
2	T51	9.74	339.5	349.9	1.03			491.5
	T53	9.74	336.0	361.6+	1.08			494.8
	T54	9.74	337.4	349.6	1.04			494.0
	T55	9.72	337.2	349.7	1.04			490.4
3	T52	9.79	333.0			359.2	1.08	
	1	9.74	331.6			364.1	1.10	
	2	9.74	334.4			362.0	1.08	
	Average	9.74	335.6	349.7	1.04	362.0	1.09	492.7

*Sources: 1 - Bethlehem Steel Corp. (Mill Test Report)
2 - Fritz Lab, Lehigh University
3 - Chicago Bridge and Iron Co.
4 - Bethlehem Steel Corporation
5 - Lukens Steel Co. (Mill Test Report)

+Values not included in average

TABLE 2A. TENSILE COUPON RESULTS

Source*	Coupon No.	Thickness (in)	Yield Stress (ksi) F_{ys}	F_{yd} 52μin/in/sec	$\frac{F_{yd}}{F_{ys}}$	F_{yd} 1042 μin/in/sec	$\frac{F_{yd}}{F_{ys}}$	F_u (ksi)
1	2	3	4	5	6	7	8	9
Specimens T2, T3, and T4: nominal ½ in plate								
1						38.0+		
2	T22	.2668	29.48	32.25	1.09			53.25
	T23	.2672	30.00	32.33	1.08			53.46
	T24	.2665	29.35	31.68	1.08			53.59
3	L7	.263	29.6	32.8	1.11	34.7	1.17	
	L8	.262	29.5	32.6	1.10	34.8	1.18	
	L9	.2635	29.4	32.7	1.11	34.5	1.17	
4	L2					38.3+		
	L3					37.4+		
	L4					40.5+		
	Average	.2648	29.56	32.40	1.10	34.67	1.17	53.43
Specimen T1: nominal 3/8 in. plate								
1						38.9		
2	T11	.3888	35.20	37.09	1.05			61.56
	T12	.3897	35.76	39.18	1.09			60.92
	T14	.3896	35.43	38.51	1.09			61.28
3	T15	.393	33.6	36.4	1.08	37.7	1.12	
	T19	.3935	34.1	37.3	1.09	39.3	1.15	
	T20	.3935	33.9	37.0	1.09	38.5	1.14	
	Average	.3914	34.67	37.58	1.08	38.5	1.14	61.25
Specimen T5: nominal 3/8 in. plate								
5						52.7		
2	T51	.3834	49.24	50.74	1.03			71.28
	T53	.3834	48.73	52.44+	1.08			71.76
	T54	.3834	48.93	50.71	1.04			71.65
	T55	.3825	48.91	50.72	1.04			71.13
3	T52	.3856	48.3			52.1	1.08	
	1	.3833	48.1			52.8	1.10	
	2	.3836	48.5			52.5	1.08	
	Average	.3836	48.67	50.72	1.04	52.5	1.09	71.46

*Sources: 1 - Bethlehem Steel Corp. (Mill Test Report)
2 - Fritz Lab, Lehigh University
3 - Chicago Bridge and Iron Co.
4 - Bethlehem Steel Corporation
5 - Lukens Steel Co. (Mill Test Report)

+Values not included in average

TABLE 3. INITIAL GEOMETRIC IMPERFECTIONS

No.	Maximum OUT-OF-ROUNDNESS			Maximum OUT-OF-STRAIGHTNESS			Type* and Location of Buckles
	$OD_{max} - OD_{min}$ (mm)	Col. 2 / OD	Location from Top (m)	Offset ** (mm)	Location from Top (m)	GL	
1	2	3	4	5	6	7	8
T1	7.60	0.0075	2.03	+1.55	1.14	8	RB-B
T2	5.56	0.0072	0.0	-3.05	0.89	9	RB-T
T3	5.94	0.0058	1.75	+2.46	1.75	2	RB-T
T4	11.71	0.0076	0.24	+1.83	1.44	2	RB-T
T5	7.75	0.0132	0.0	-2.21	0.80	1	W,RB-B
P11	18.29	0.0119	1.96	+2.36	0.33	13	DB-T,M

*Type and location of buckling failure:
RB-T = Ring bulge at top of specimen
RB-B = Ring bulge at bottom
W = Wave-like pattern along length
DB-T,M = Diamond-shaped buckles at top and middle
**A negative offset is inward, a positive is outward
GL = Gage Line

TABLE 3A. INITIAL GEOMETRIC IMPERFECTIONS

No.	Maximum OUT-OF-ROUNDNESS			Maximum OUT-OF-STRAIGHTNESS			Type * and loc. of buckles
	$OD_{max}-OD_{min}$ (in.)	Col. 2 / OD	Location from top (in.)	Offset ** (in.)	Location from top (in.)	GL	
1	2	3	4	5	6	7	8
T1	0.229	0.0075	80.0	+0.061	45.1	8	RB-B
T2	0.219	0.0072	0.0	-0.120	35.1	9	RB-T
T3	0.234	0.0058	68.9	+0.097	68.9	2	RB-T
T4	0.461	0.0076	9.4	+0.072	56.9	2	RB-T
T5	0.305	0.0132	0.0	-0.087	31.5	1	W,RB-B
P11	0.720	0.0119	77.0	+0.093	13.0	13	DB-T,M

* Type and location of buckling failure:
RB-T = Ring bulge at top of specimen
RB-B = Ring bulge at bottom
W = Wave-like pattern along length
DB-T,M = Diamond-shaped buckles at top and middle
** A negative offset is inward, a positive is outward
GL = Gage Line

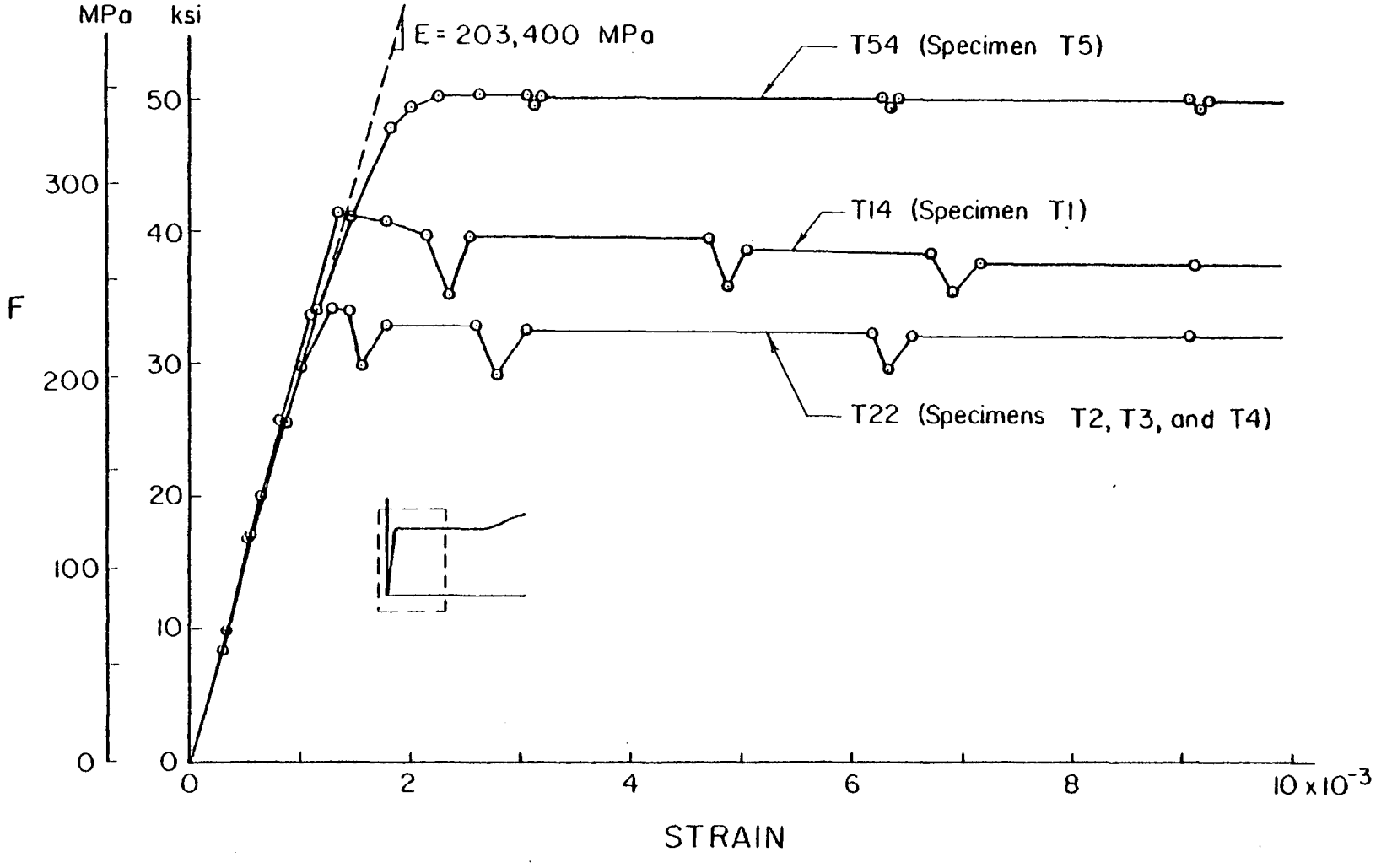

Fig. 1 Typical A36 Coupon Stress-Strain Curves for Strains Less Than 0.010

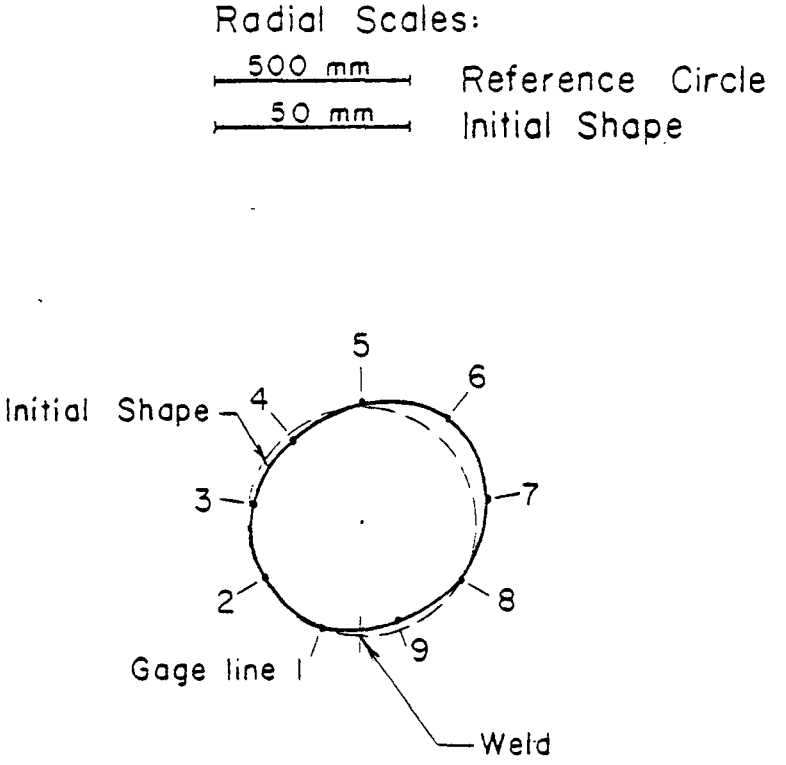

Fig. 2 Initial Out-of-Roundness and Location of Gage Lines in Specimen T5 ($D/t = 59.1$, $F_{ys} = 336$ MPa)

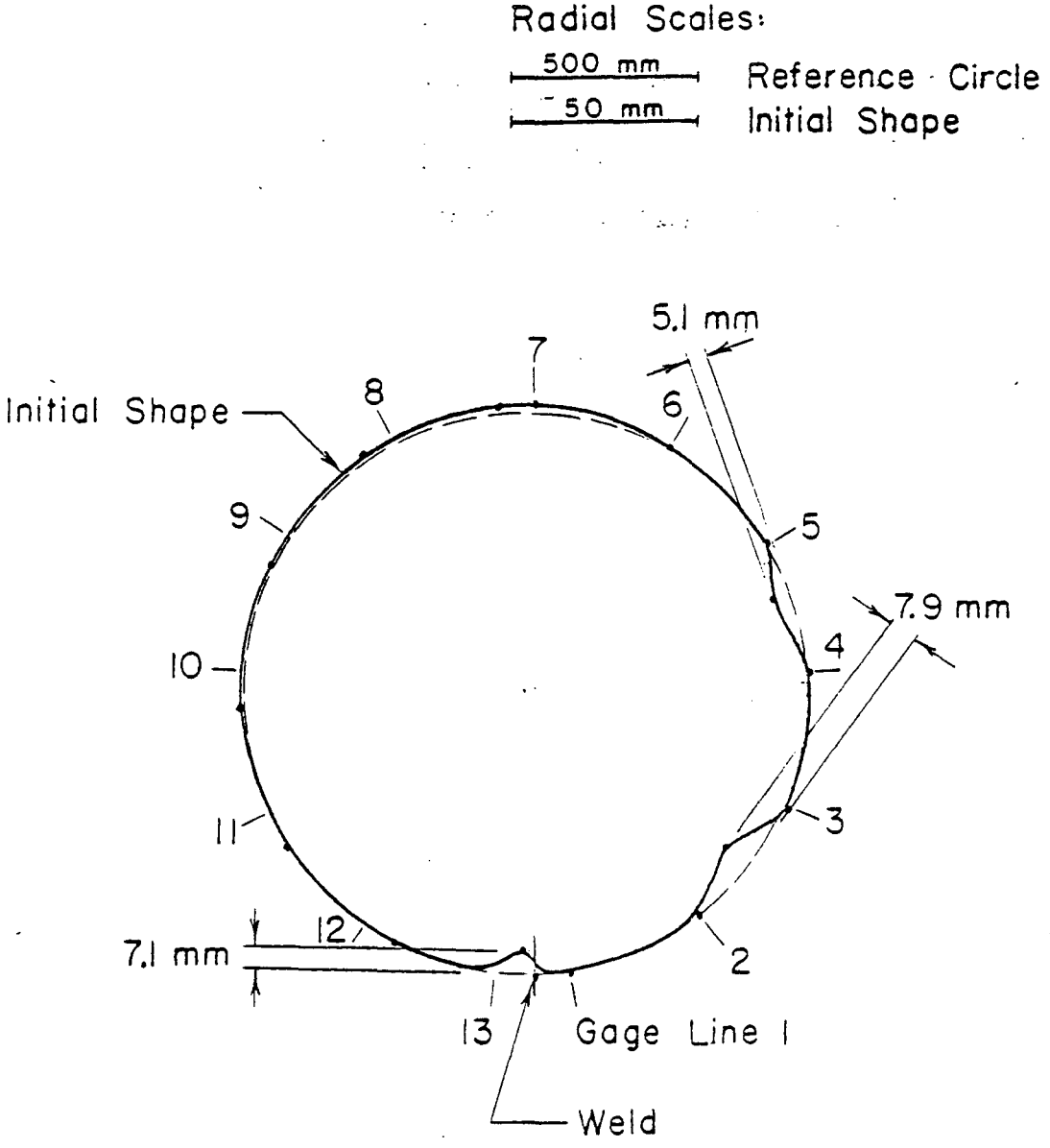

Fig. 3 Local Imperfections and Location of Gage Lines in Specimen P11 ($D/t = 233$, $F_{ys} = 623$ MPa)

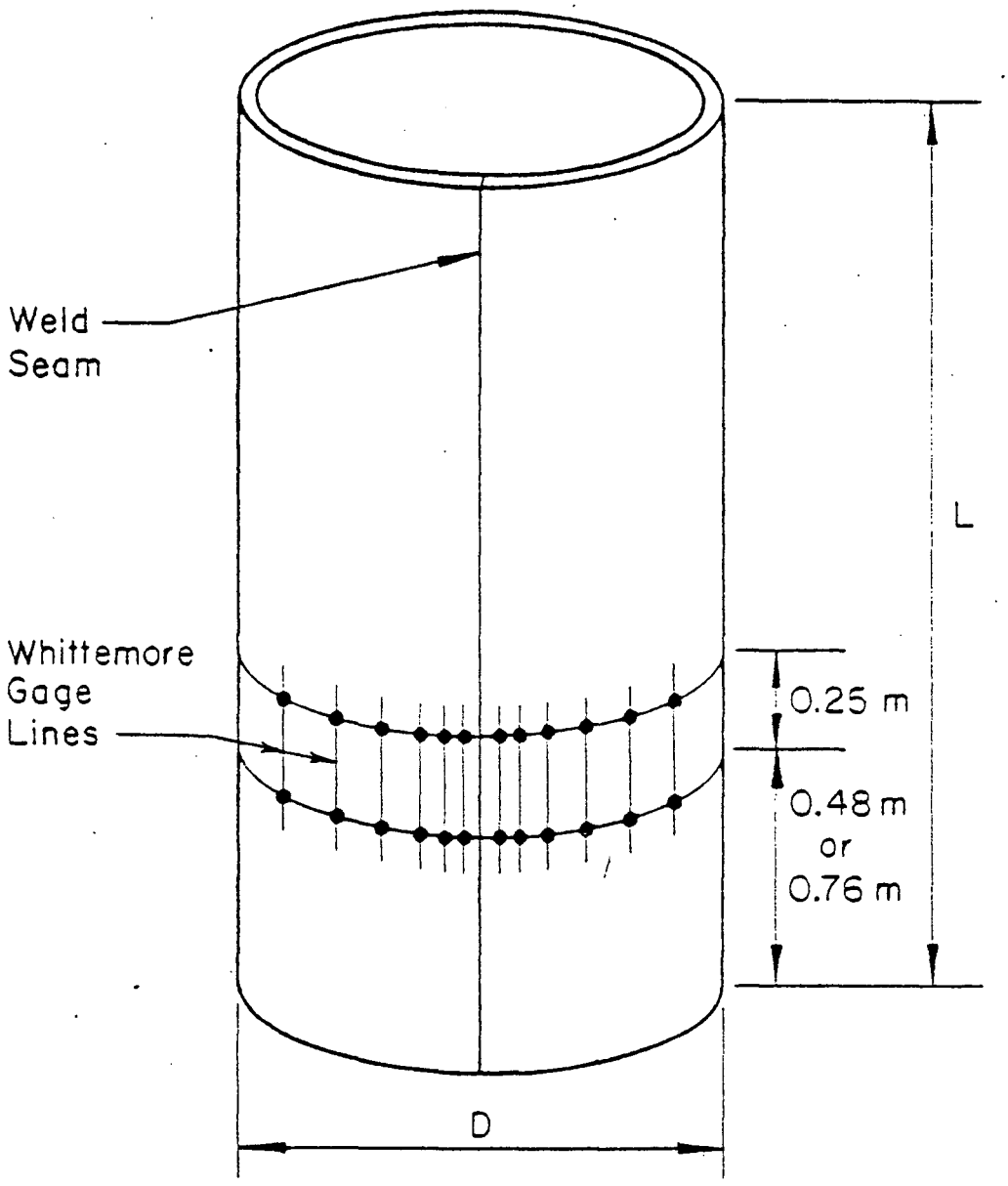

Fig. 4 Residual Stress Measurement Hole Locations

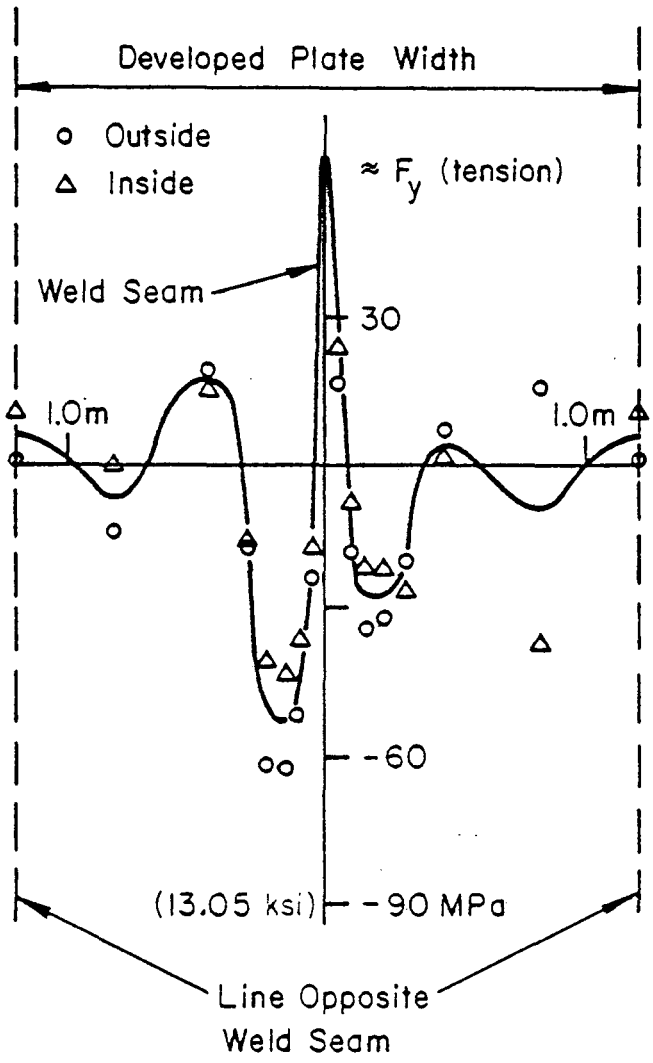

Fig. 5 Residual Stress Distribution in Specimen T2
(D/t = 113, F_{ys} = 204 MPa)

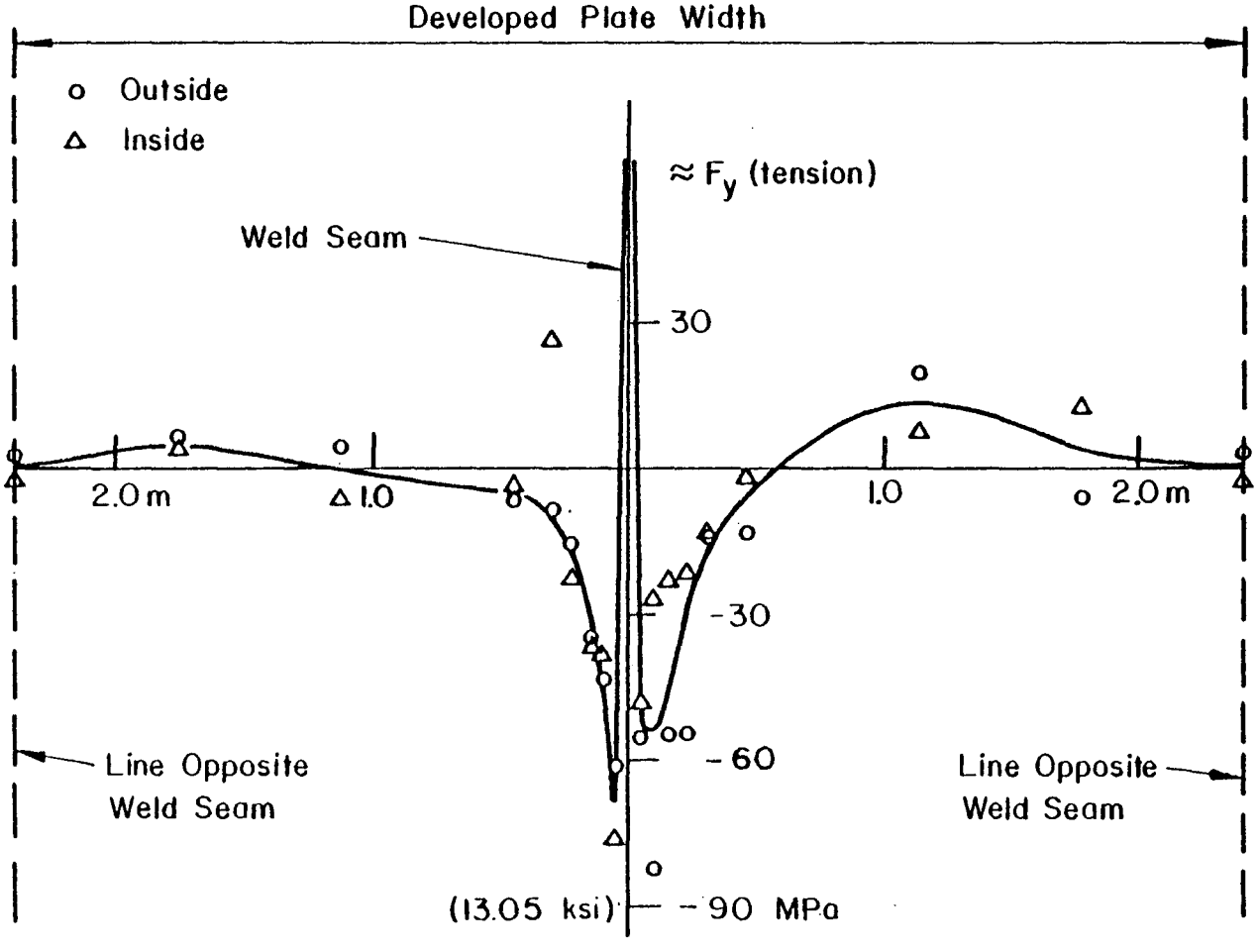

Fig. 6 Residual Stress Distribution in Specimen T4
(D/t = 227, F_{ys} = 204 MPa)

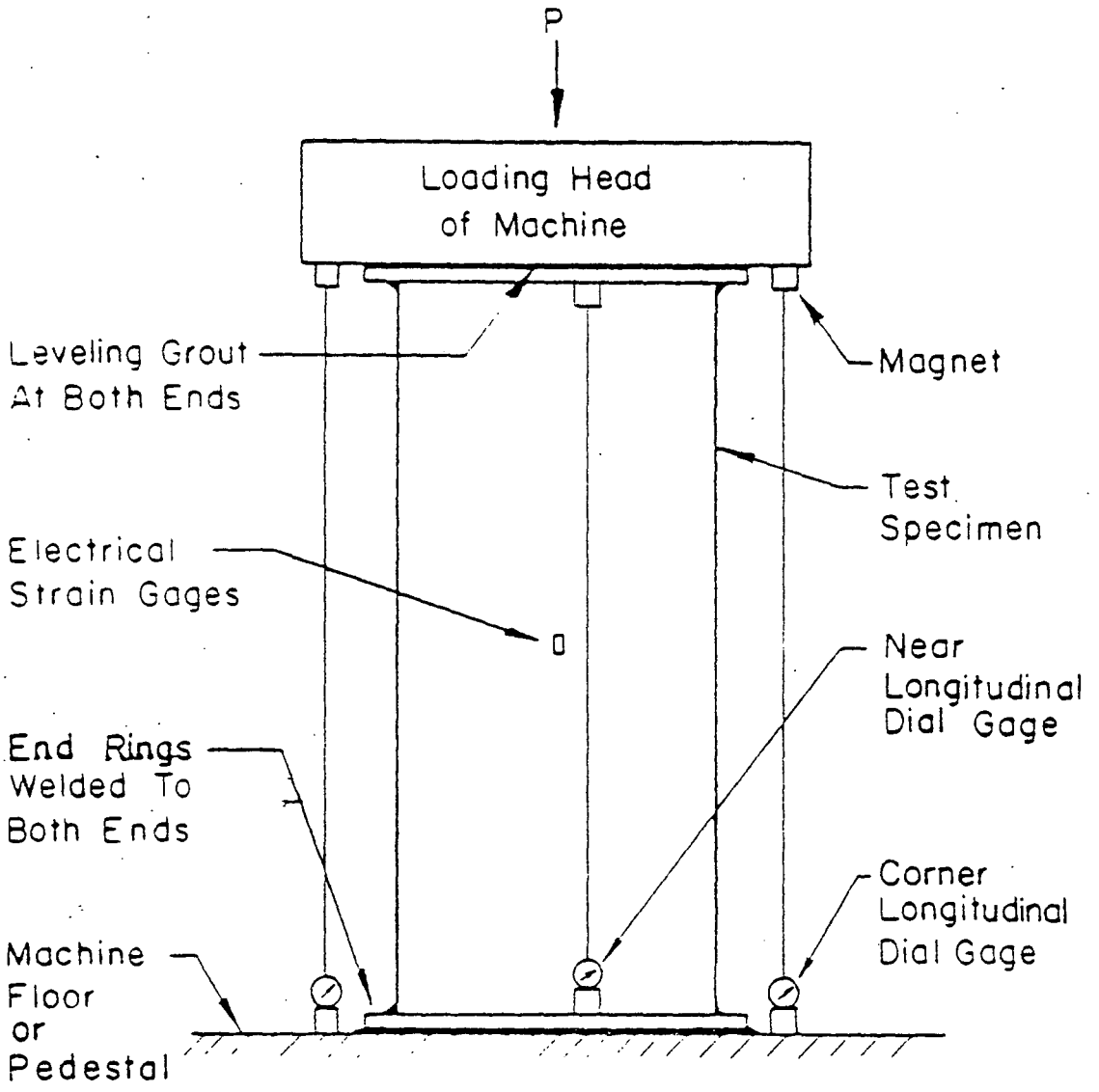

Fig. 7 Schematic of General Test Setup

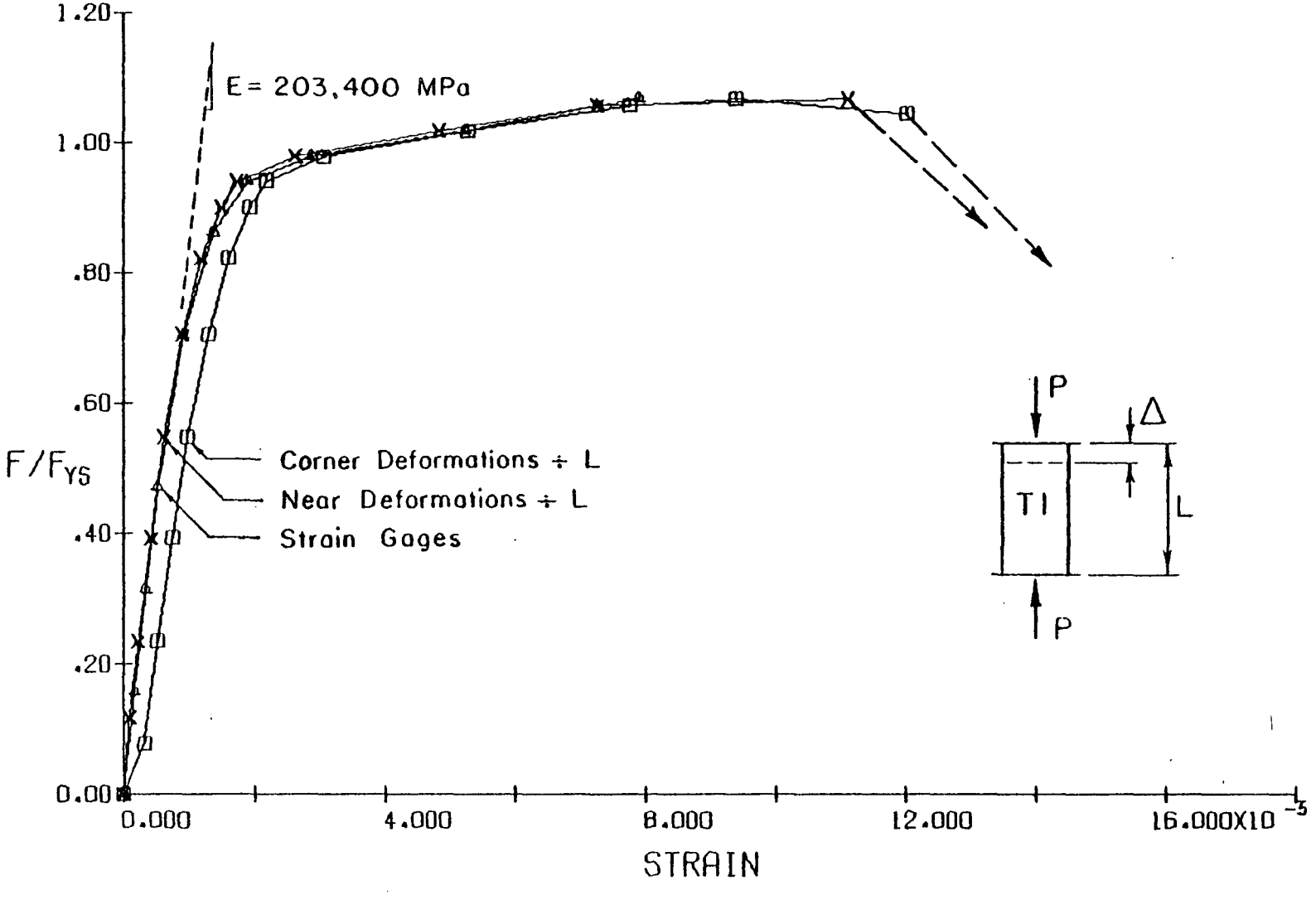

Fig. 8 Stress-Strain Curve for T1
($D/t = 77$, $F_{ys} = 239$ MPa)

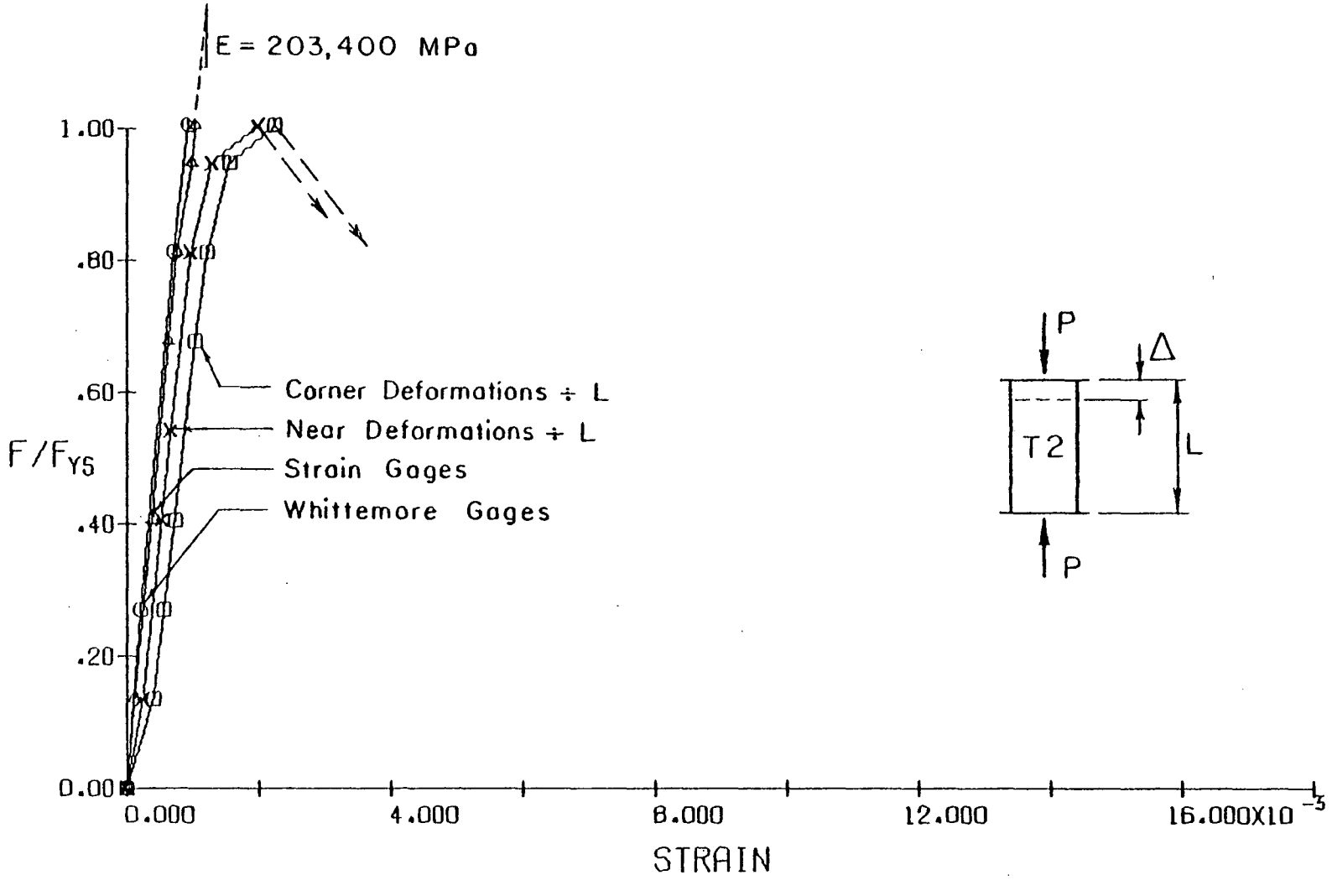

Fig. 9 Stress-Strain Curve for T2
(D/t = 113, F_{ys} = 204 MPa)

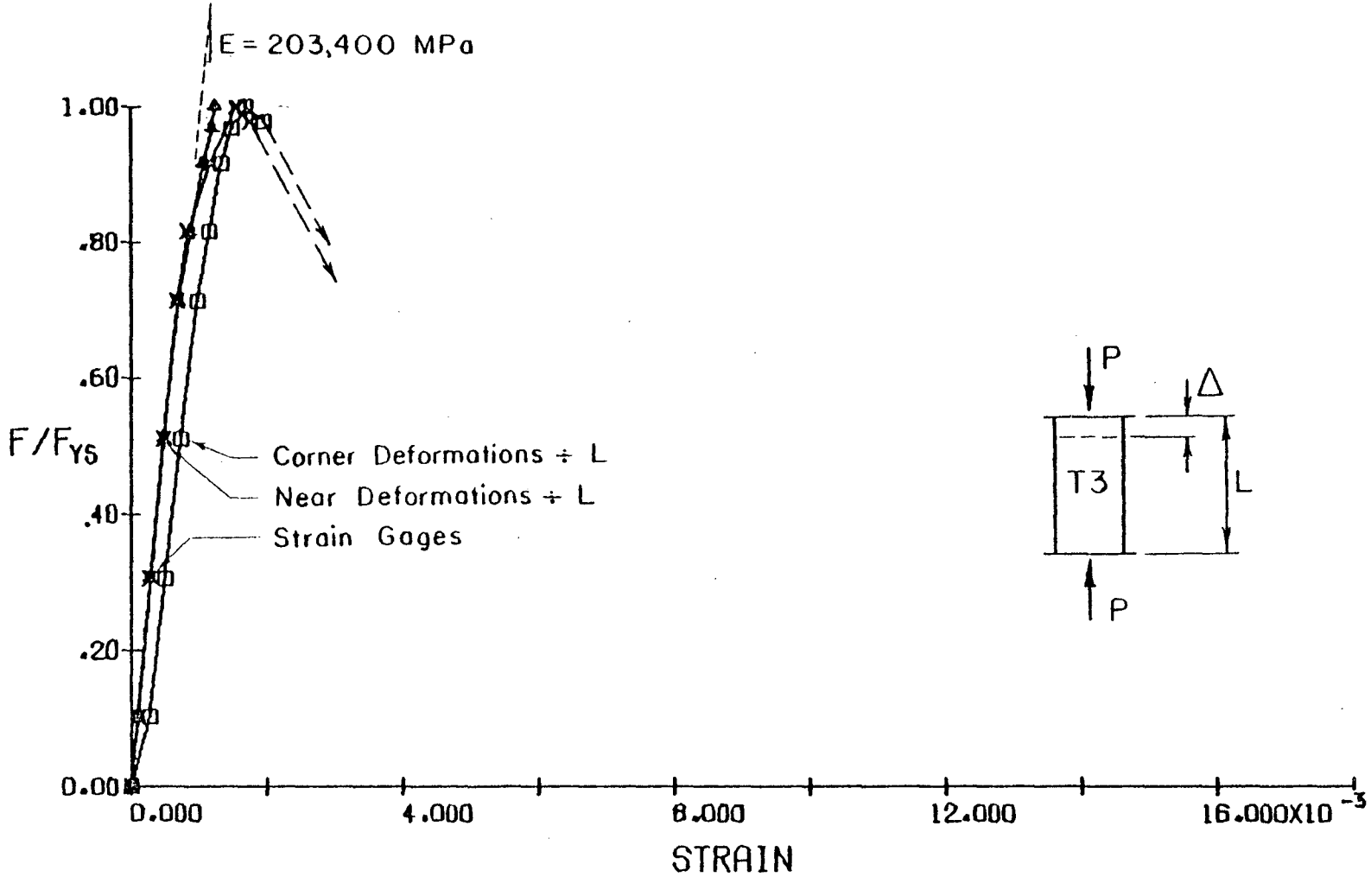

Fig. 10 Stress-Strain Curve for T3
($D/t = 151$, $F_{ys} = 204$ MPa)

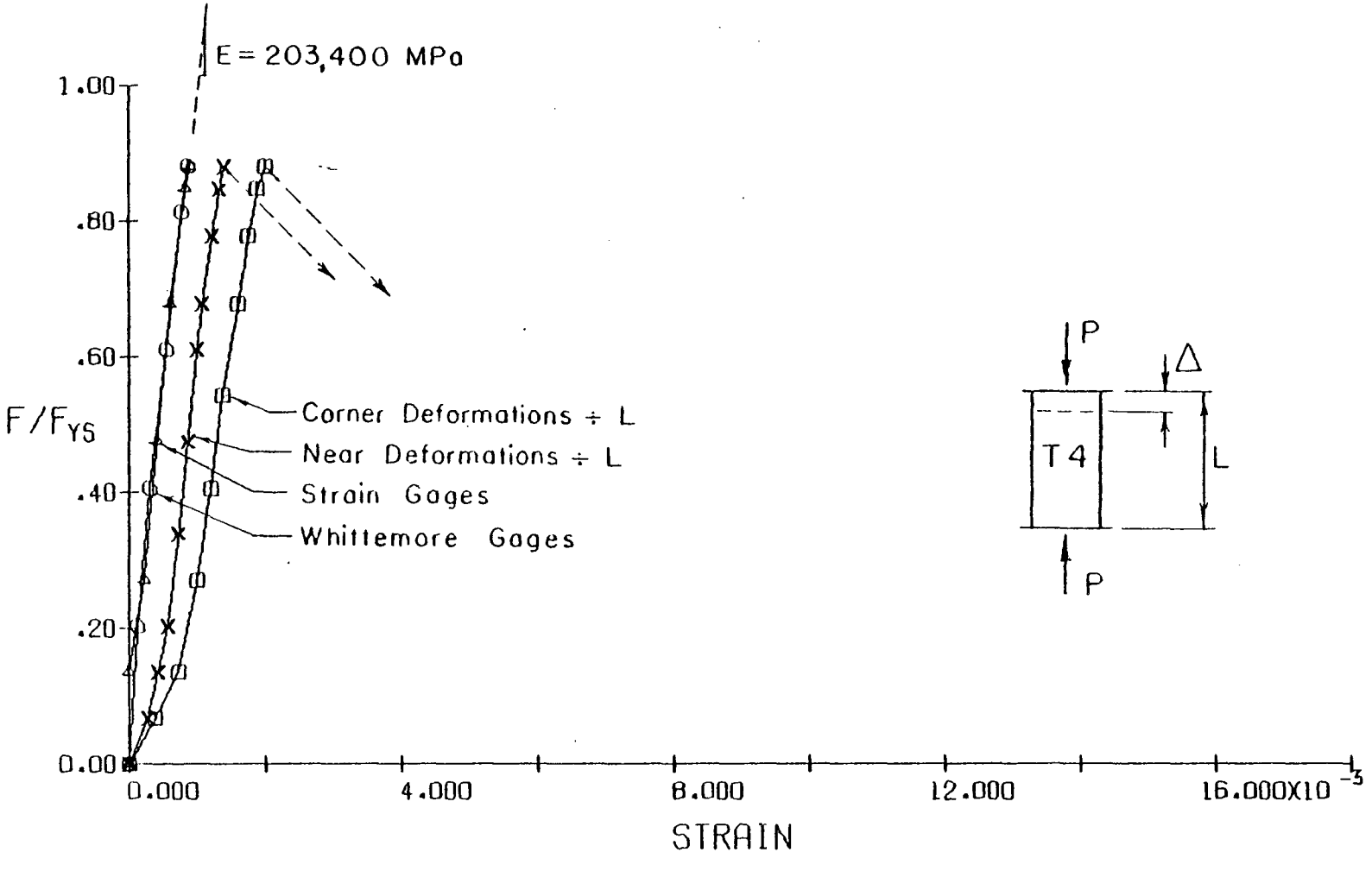

Fig. 11 Stress-Strain Curve for T4
(D/t = 227, F_{ys} = 204 MPa)

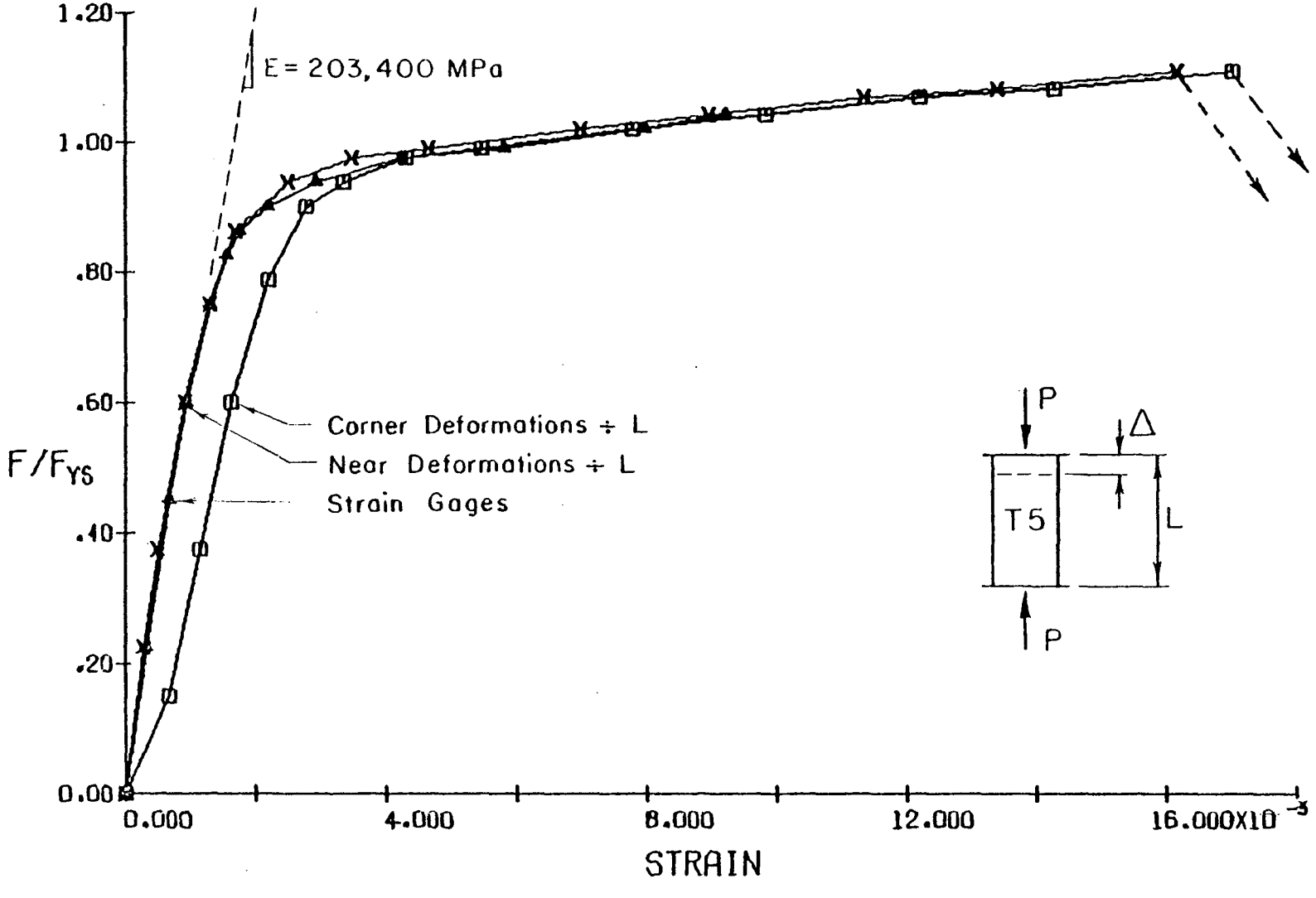

Fig. 12 Stress-Strain Curve for T5
($D/t = 59$, $F_{ys} = 336$ MPa)

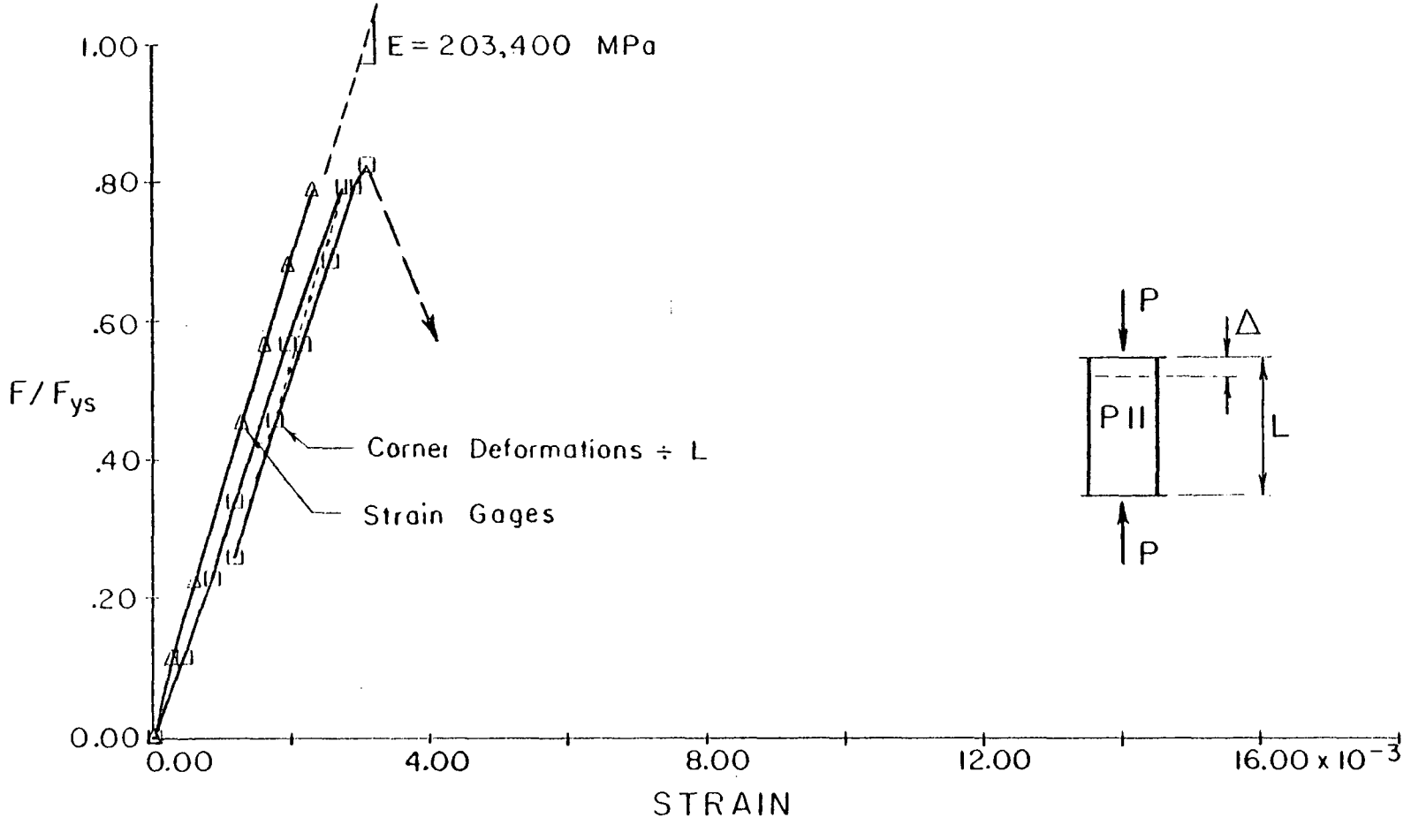

Fig. 13 Stress-Strain Curve for P11
(D/t = 233, F_{ys} = 623 MPa)

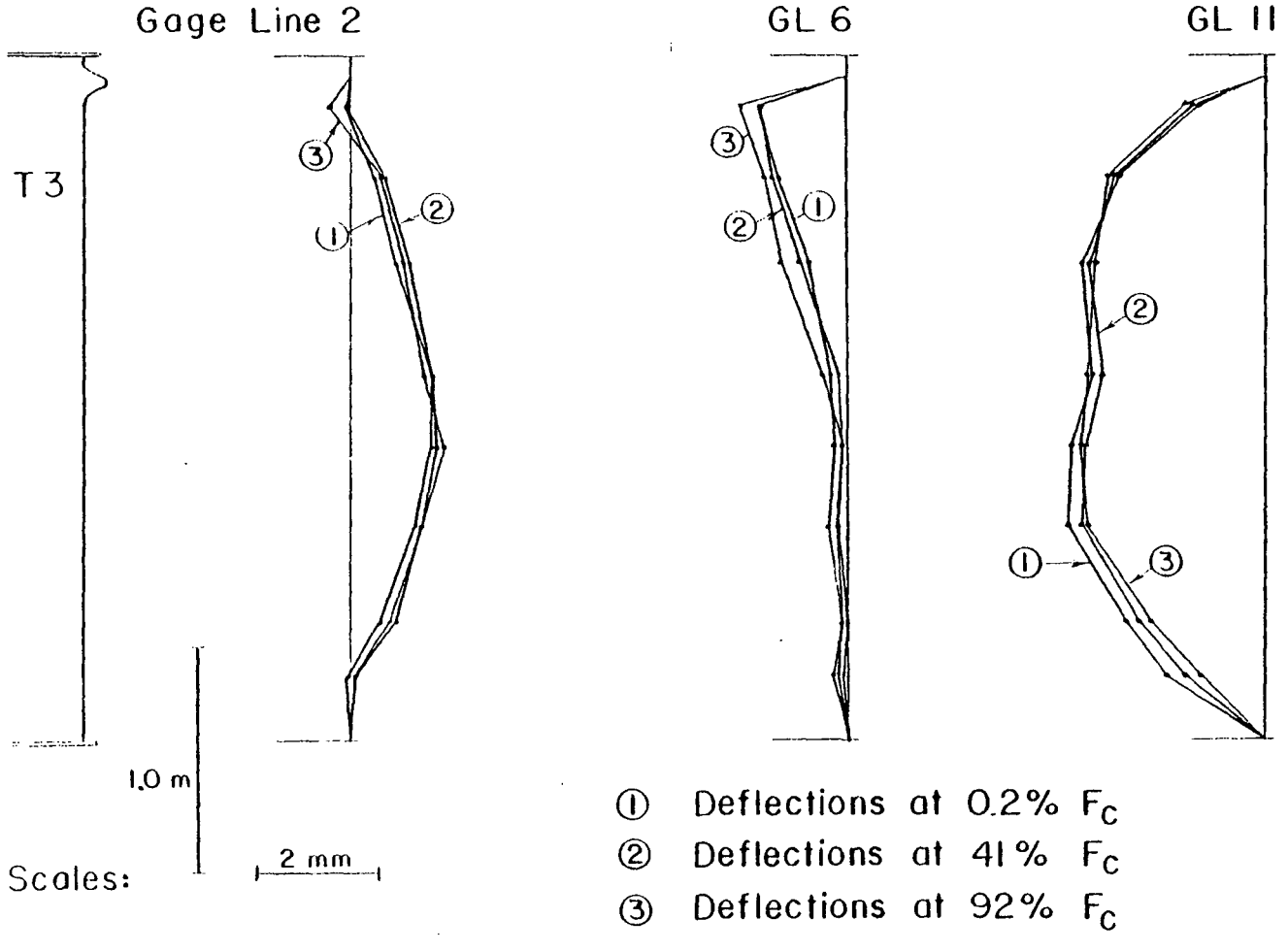

Fig. 14 Lateral Deflection Profiles for T3

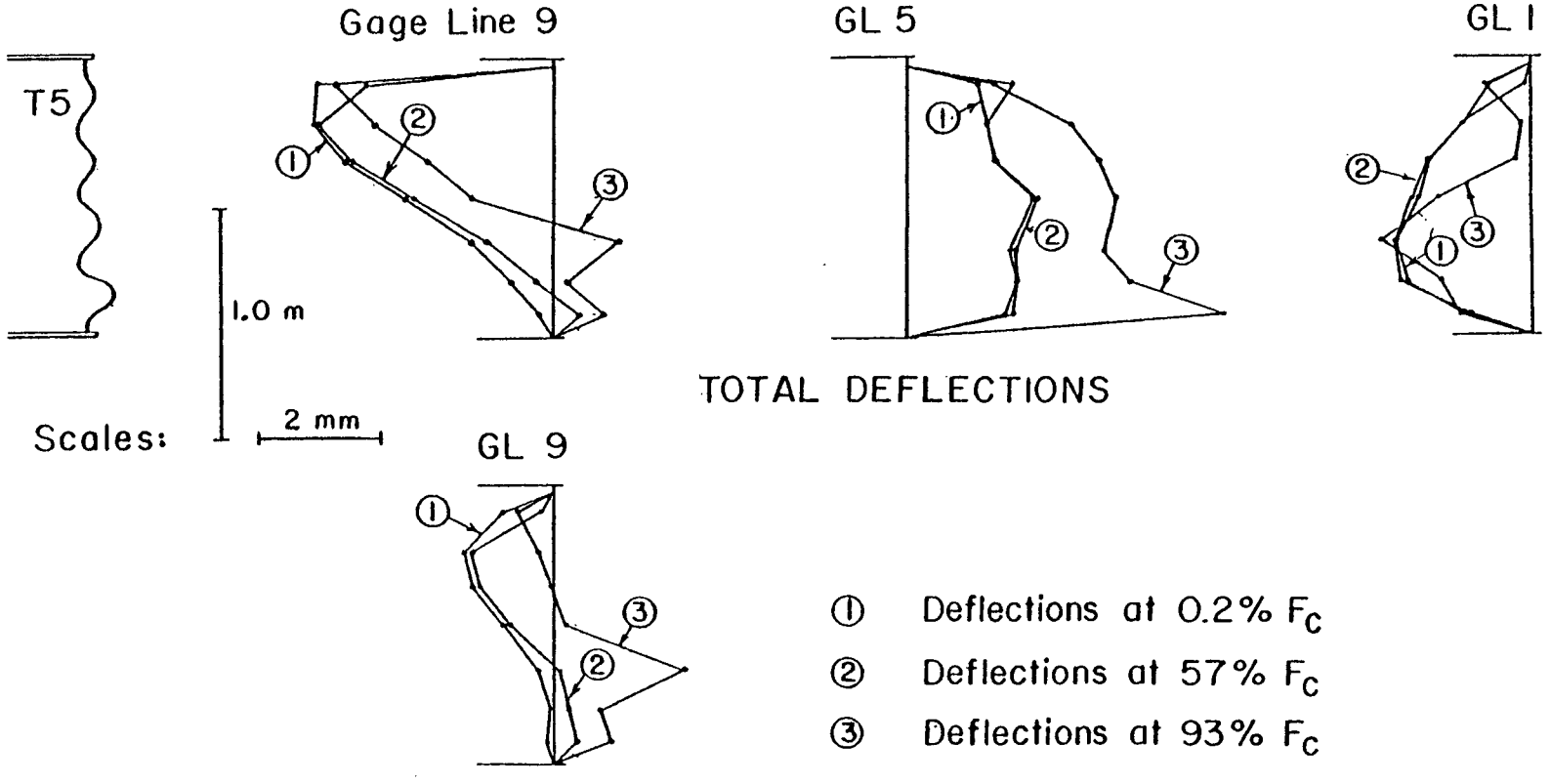

Fig. 15 Lateral Deflection Profiles for T5

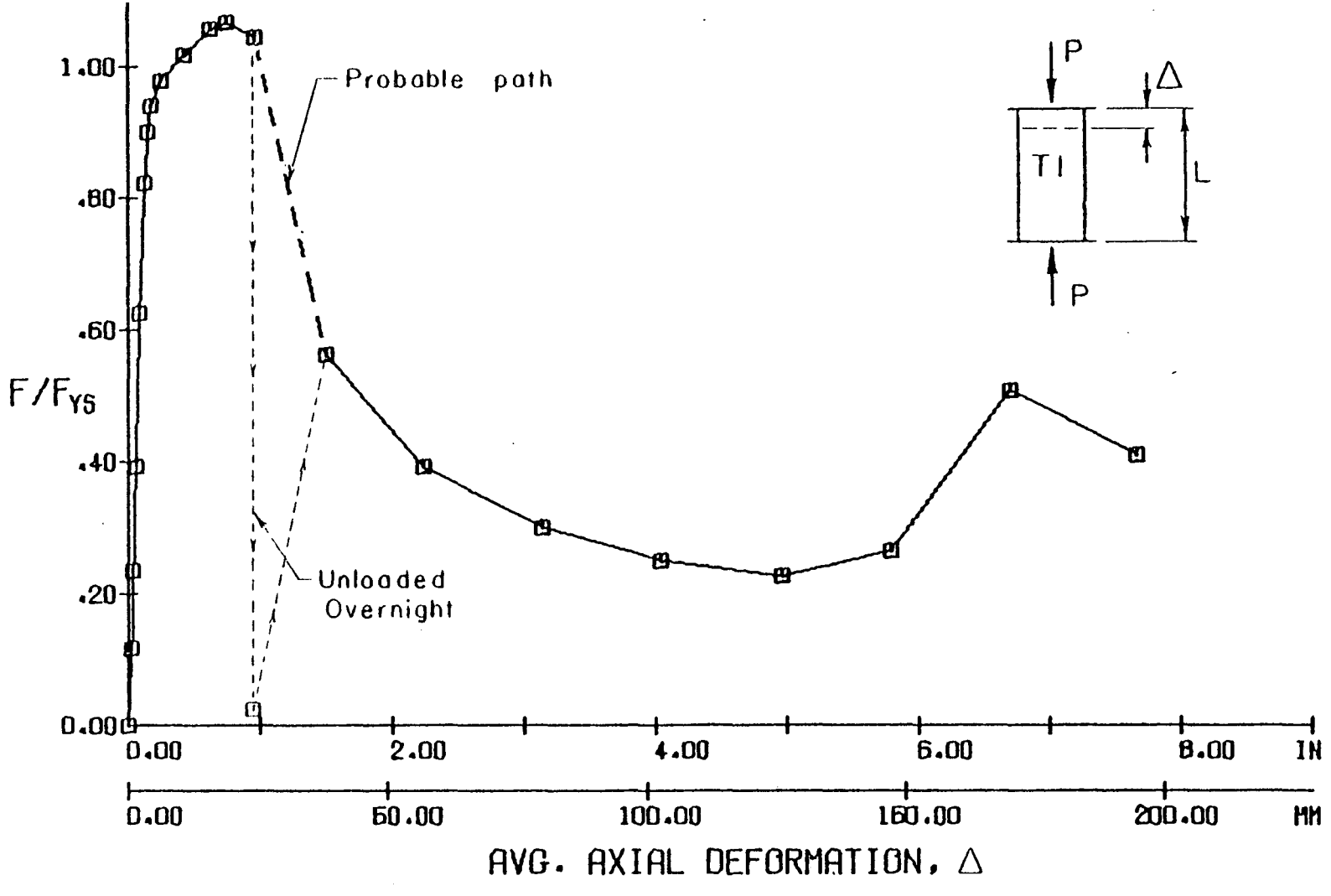

Fig. 16 Stress-Deformation Curve for T1
($D/t = 77$, $F_{ys} = 239$ MPa)

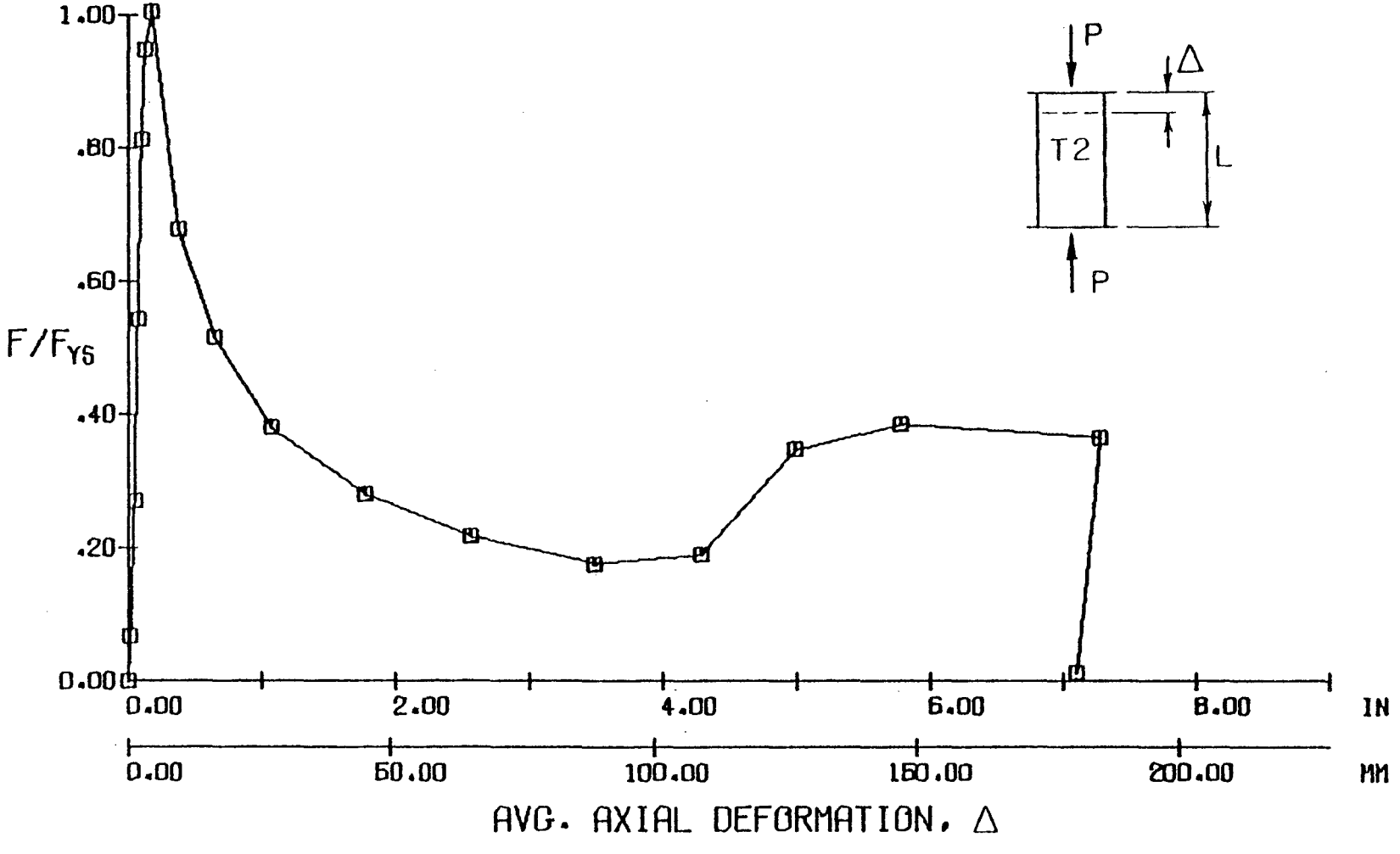

Fig. 17 Stress-Deformation Curve for T2
(D/t = 113, F_{ys} = 204 MPa)

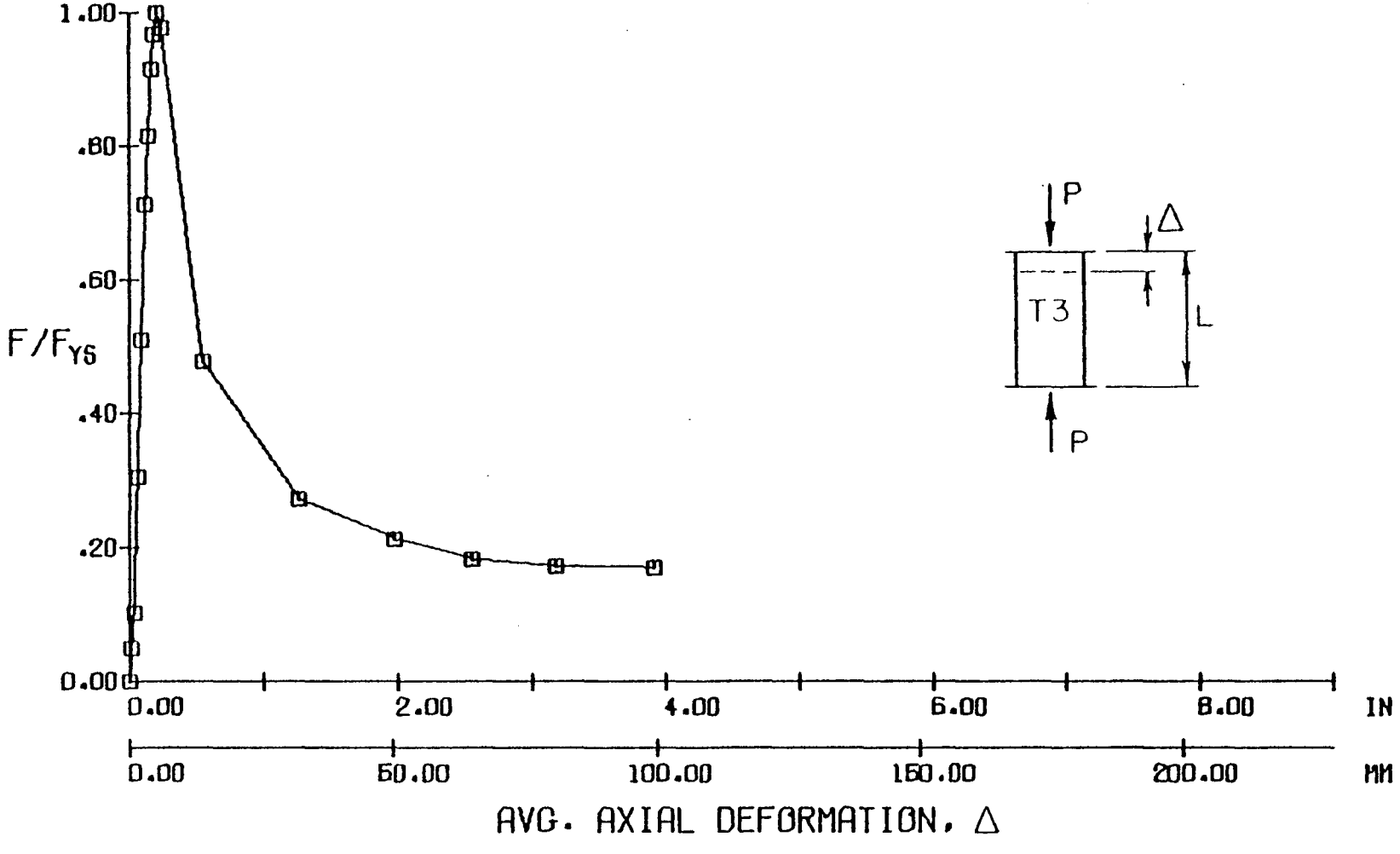

Fig. 18 Stress-Deformation Curve for T3
($D/t = 151$, $F_{ys} = 204$ MPa)

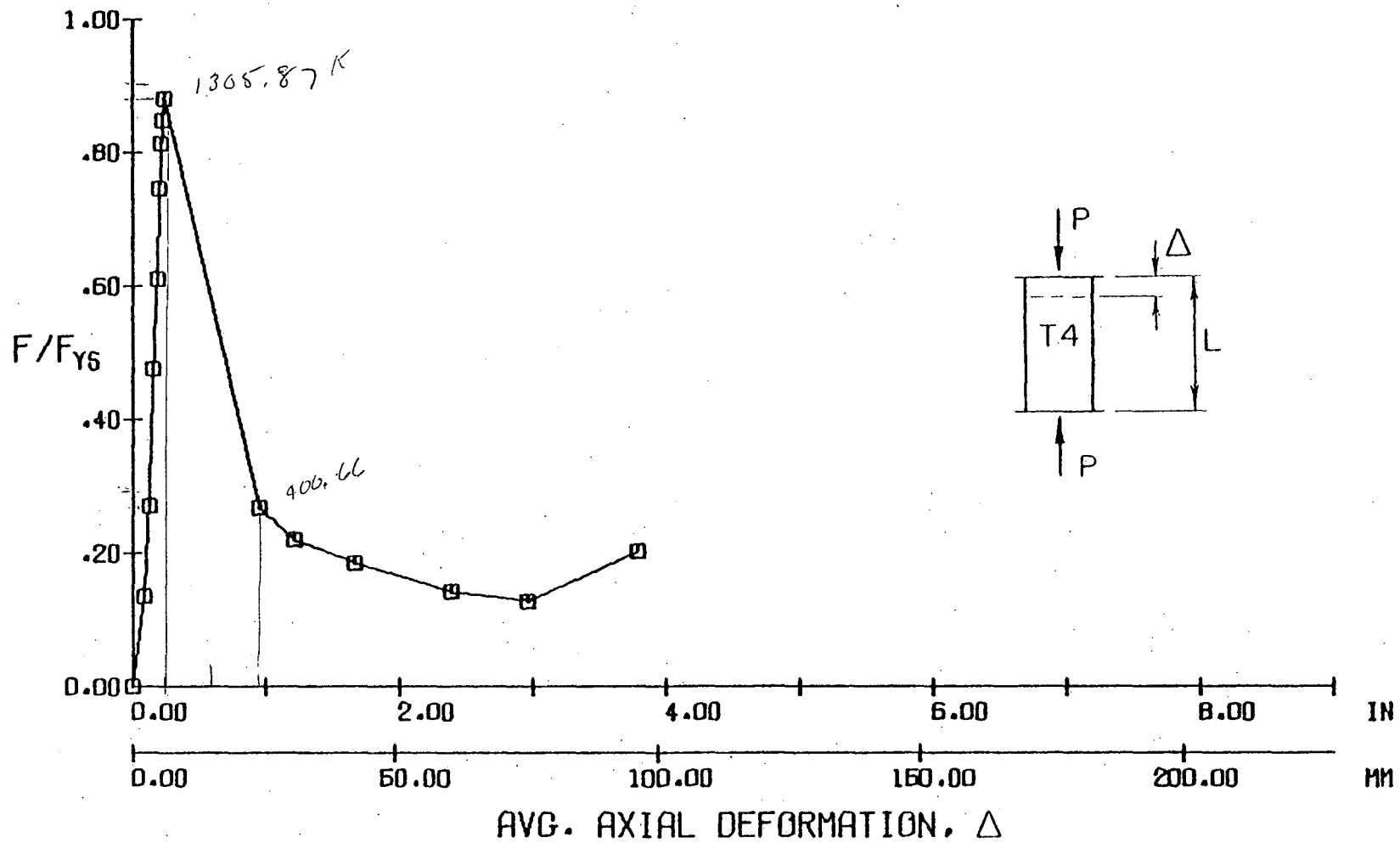

Fig. 19 Stress-Deformation Curve for T4
(D/t = 227, F_{ys} = 204 MPa)

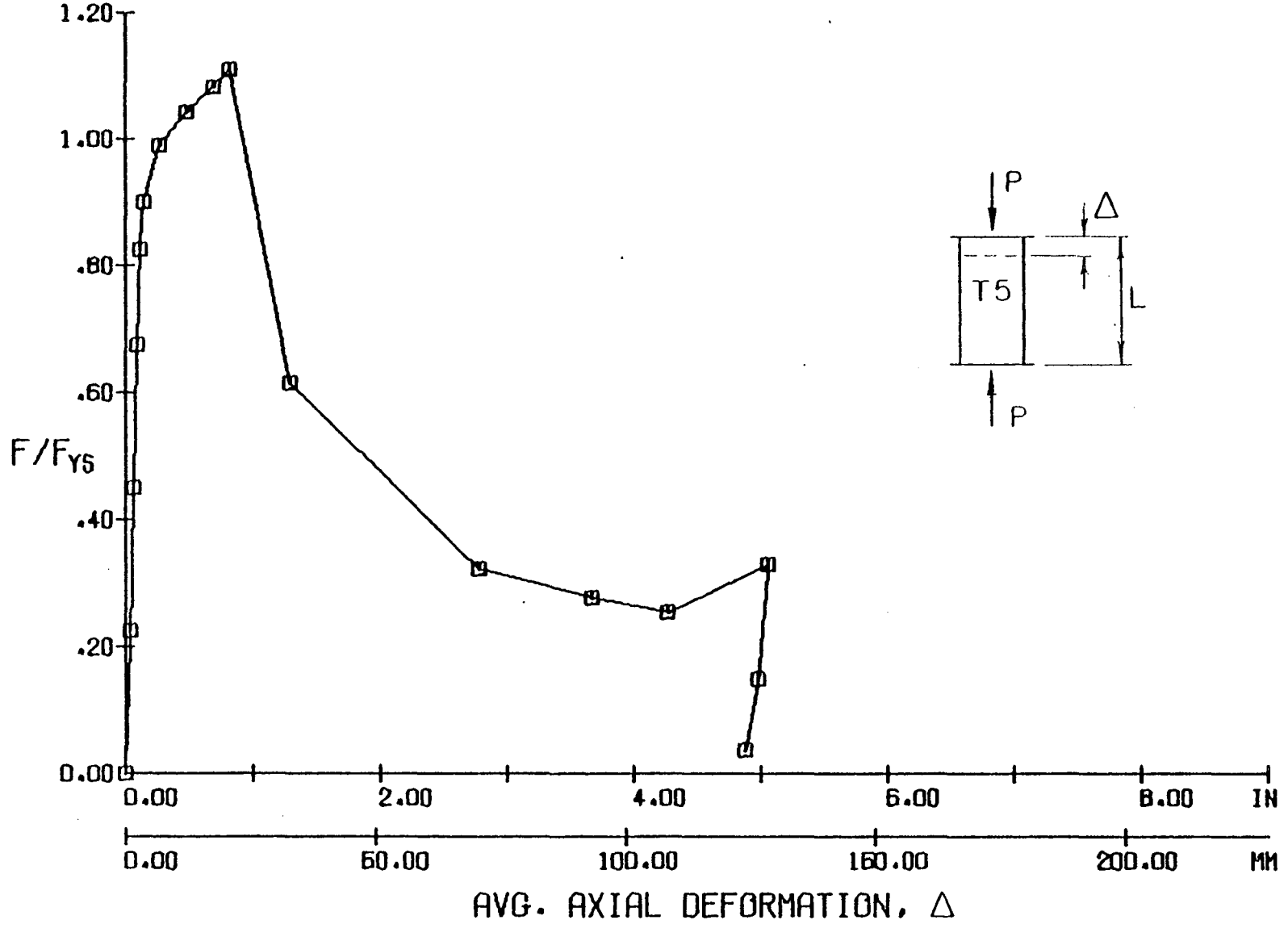

Fig. 20 Stress-Deformation Curve for T5
($D/t = 59$, $F_{ys} = 336$ MPa)

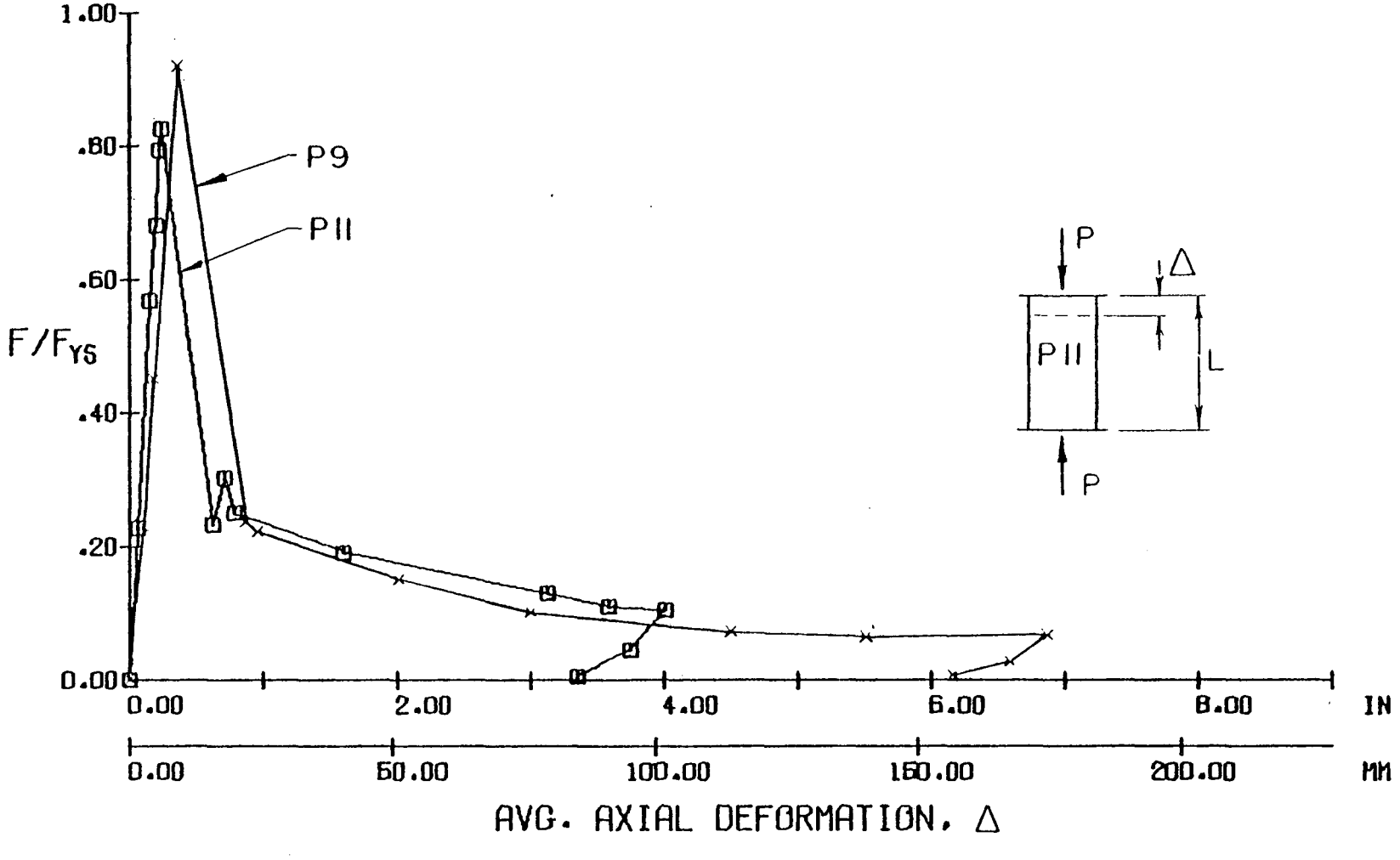

Fig. 21 Stress-Deformation Curves for P11 and P9
($D/t = 233$, $F_{ys} = 623$ MPa)

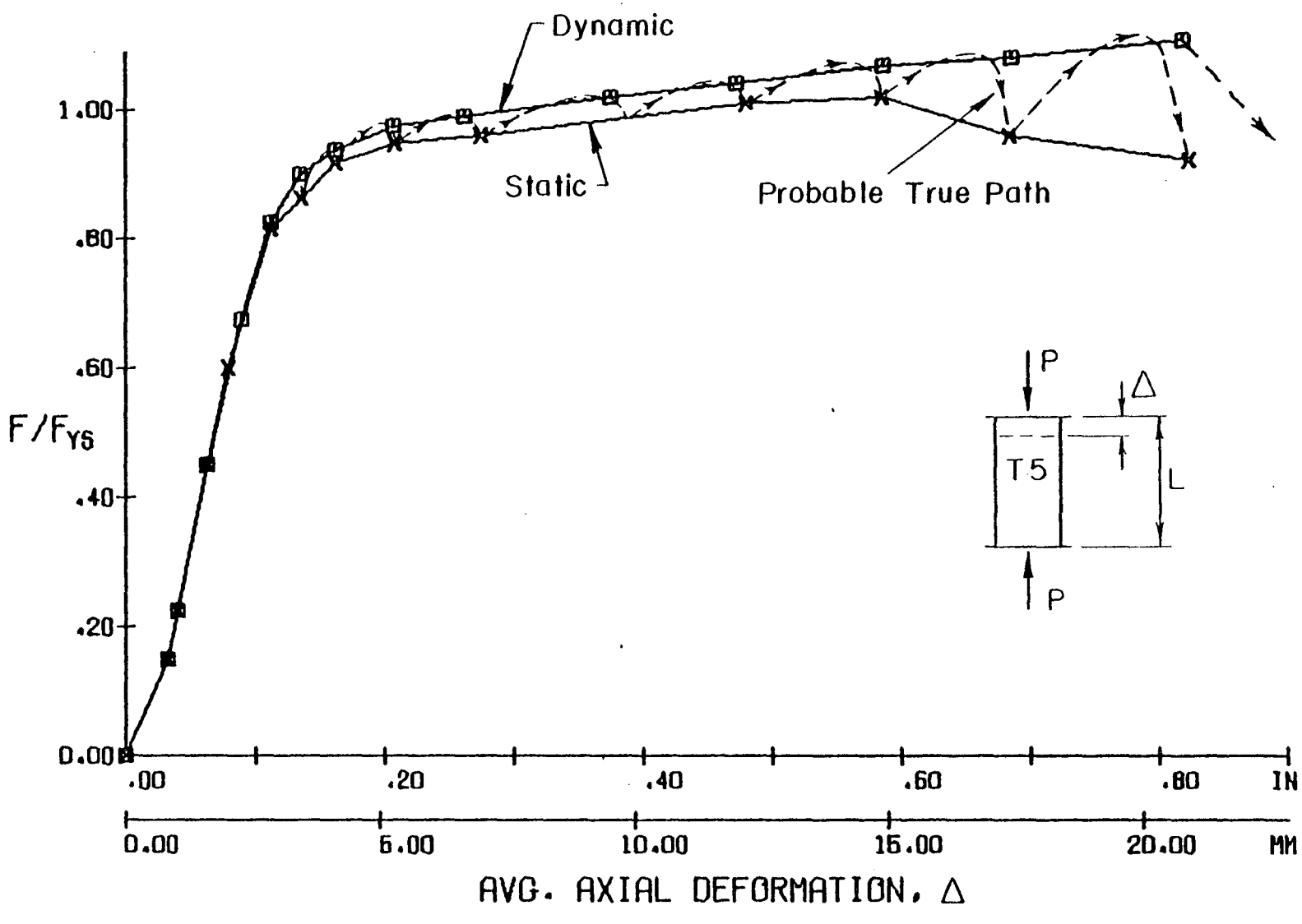

Fig. 22 Expanded Scale Stress-Deformation Curve for T5 ($D/t = 59$, $F_{ys} = 336$ MPa)

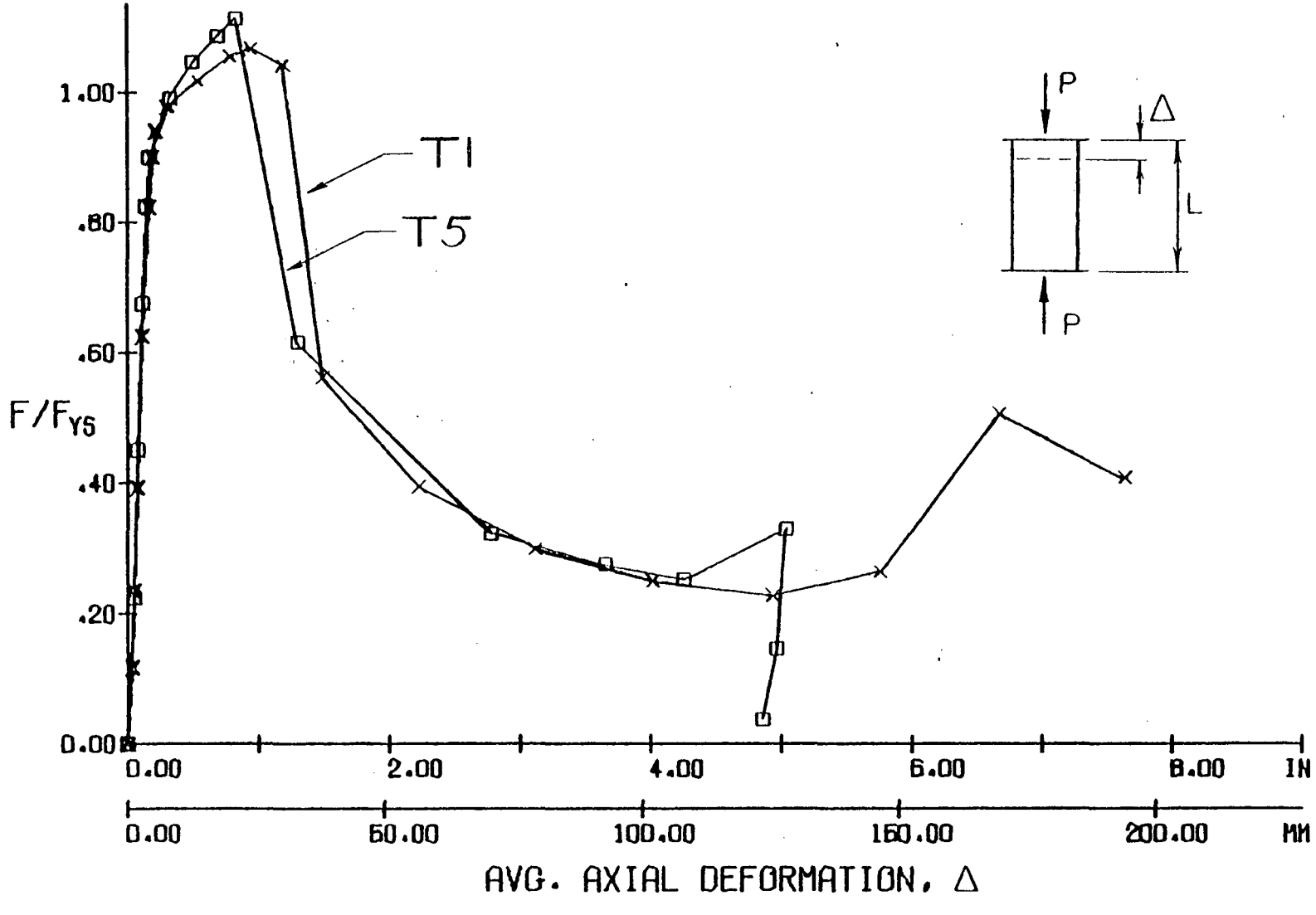

Fig. 23 Comparison of Stress-Deformation Curves for T1 and T5

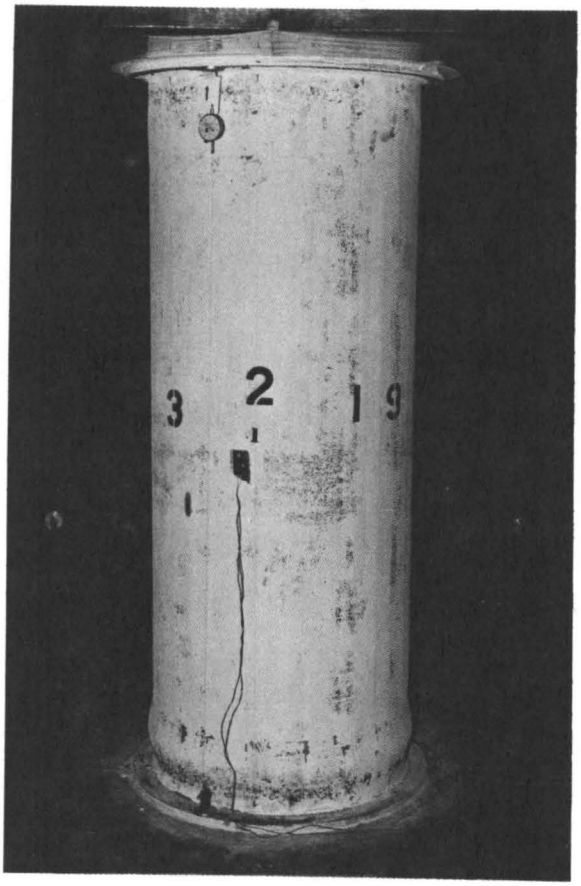

Fig. 24 Extensive Yielding in T1

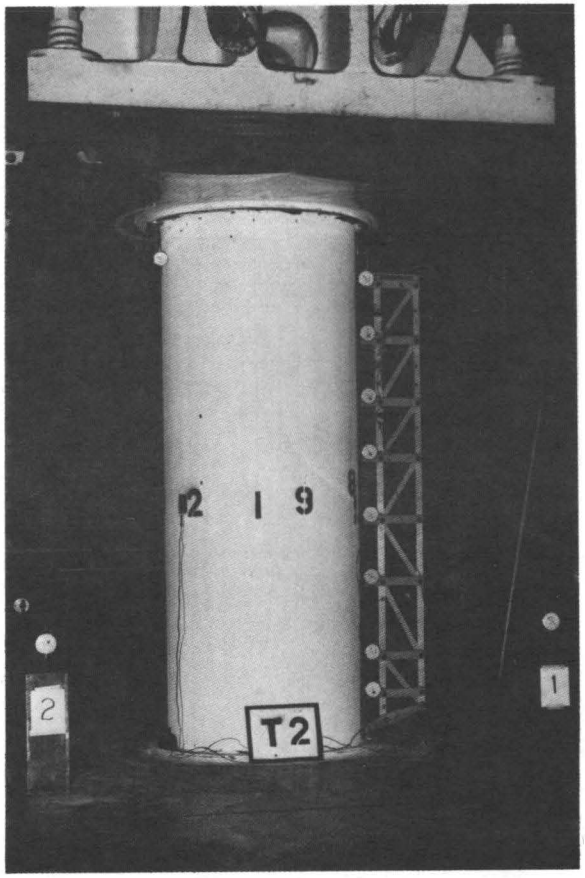

Fig. 25 Test Setup for T2

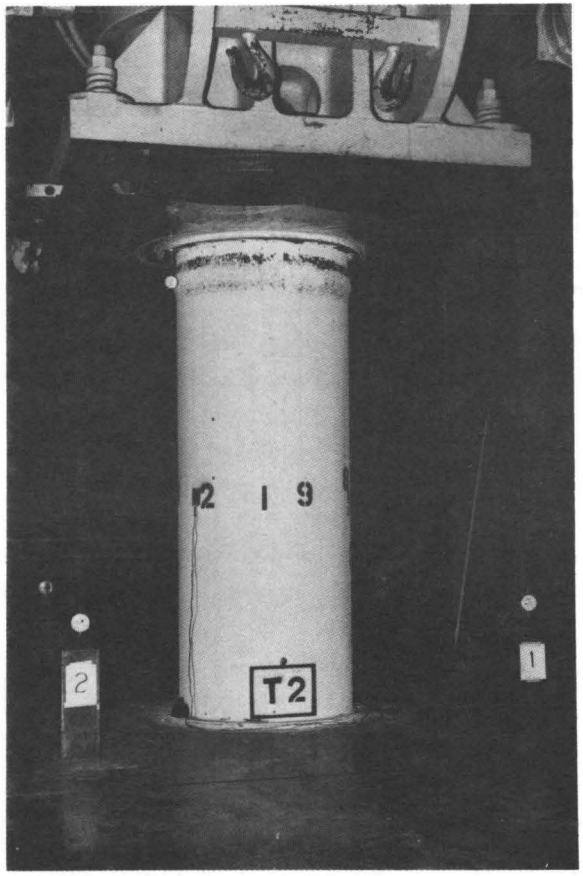

Fig. 26 Overall View of T2 after Formation of Ring Bulge

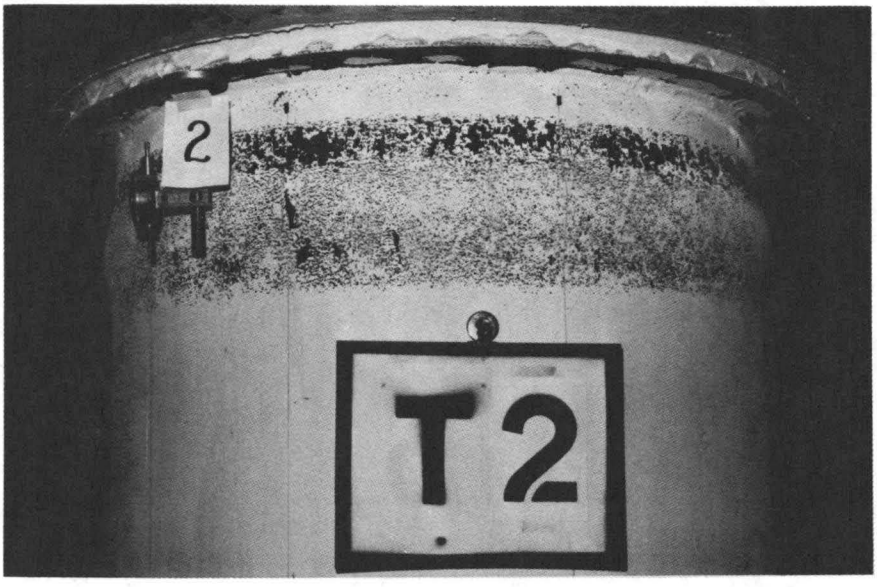

Fig. 27 Close-up of Ring Bulge in T2

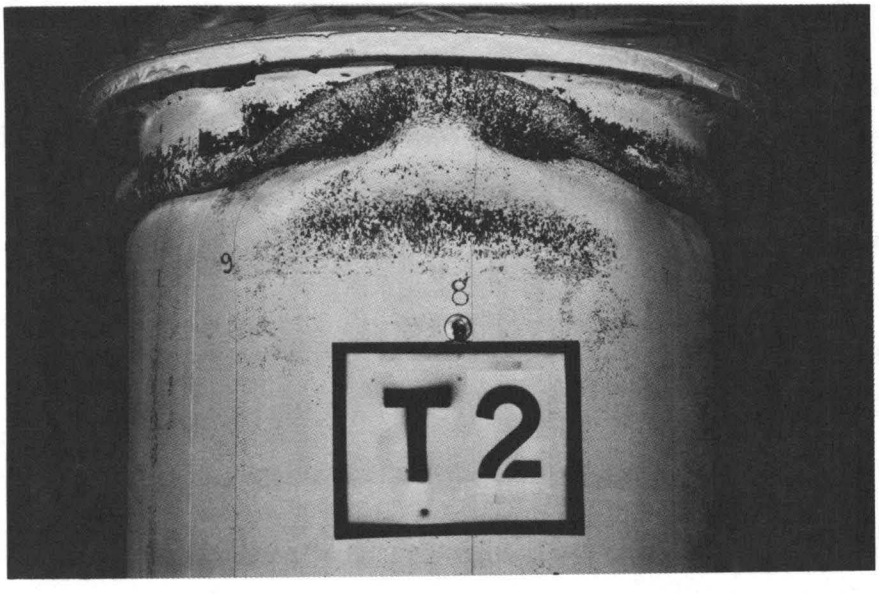

Fig. 28 Post-Buckling Deformations in T2

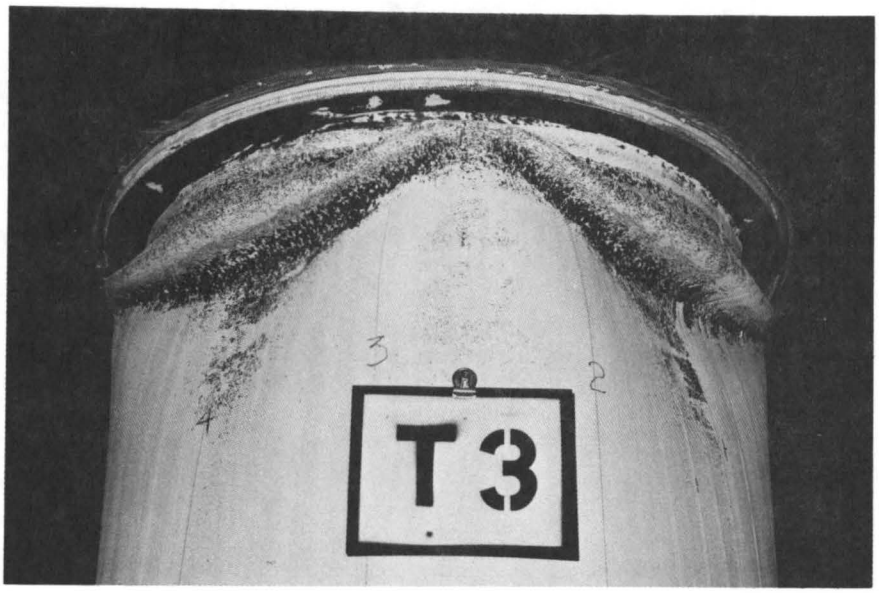

Fig. 29 Post-Buckling Deformations in T3

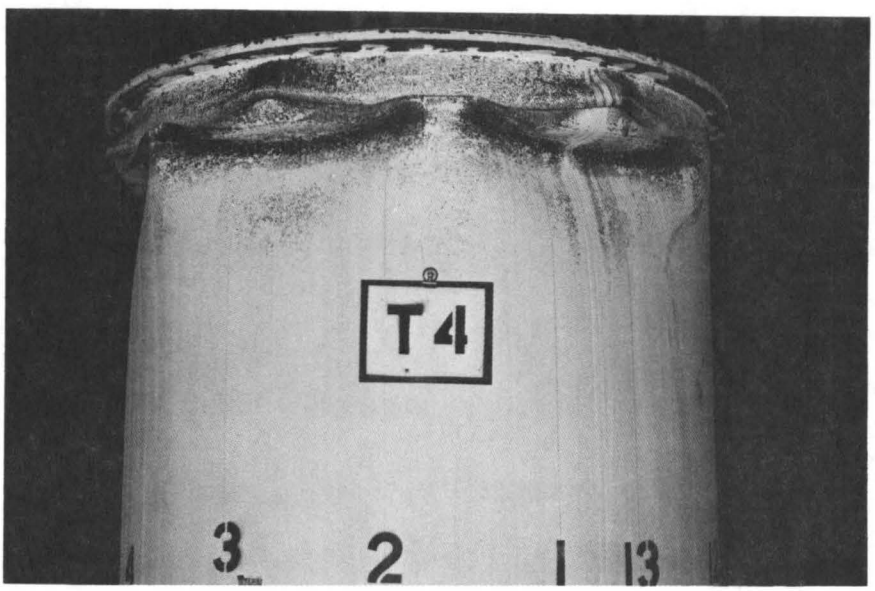

Fig. 30 Post-Buckling Deformations in T4

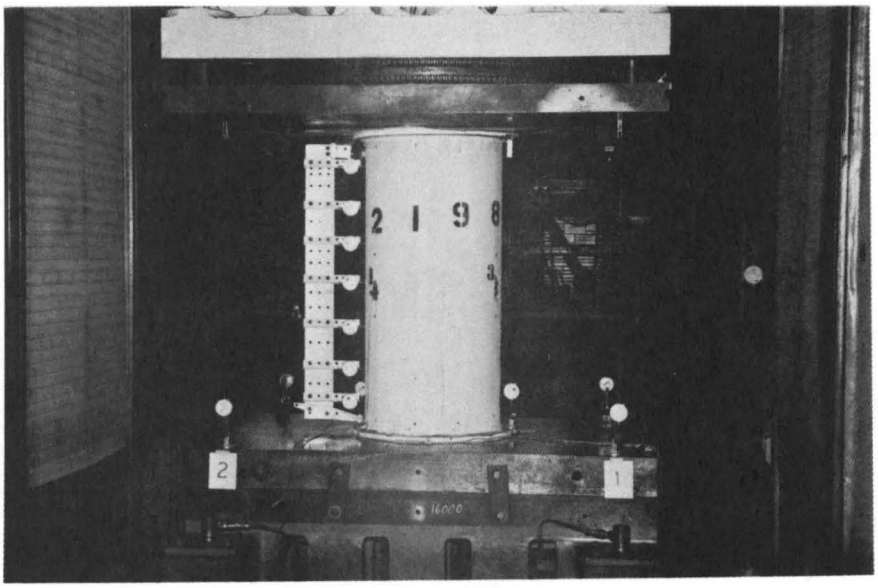

Fig. 31 Test Setup for T5

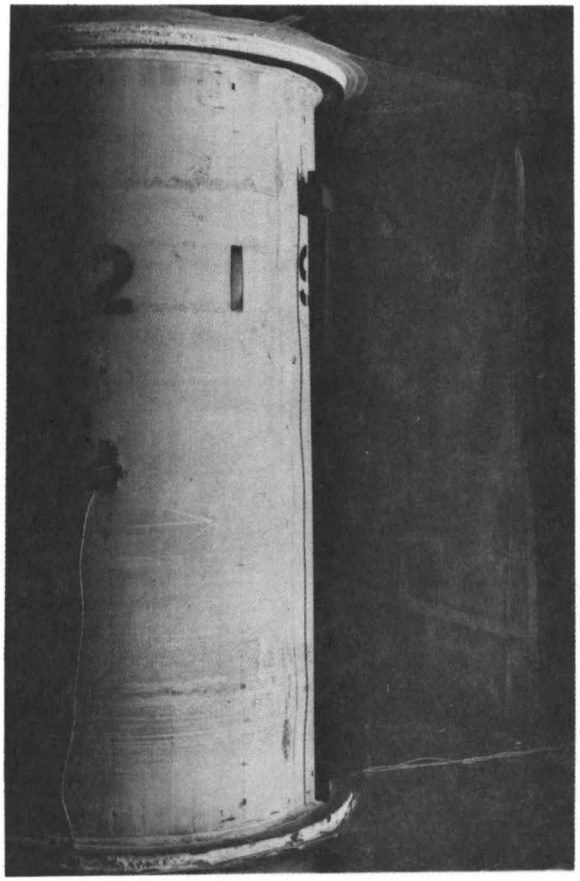

Fig. 32 Longitudinal Wave-Like Buckles in T5

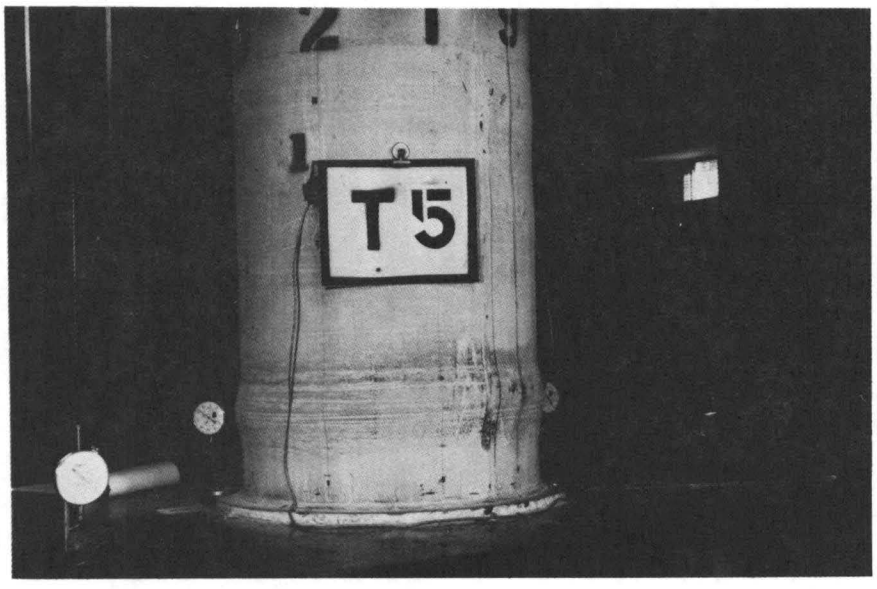

Fig. 33 Formation of Ring Bulge in T5

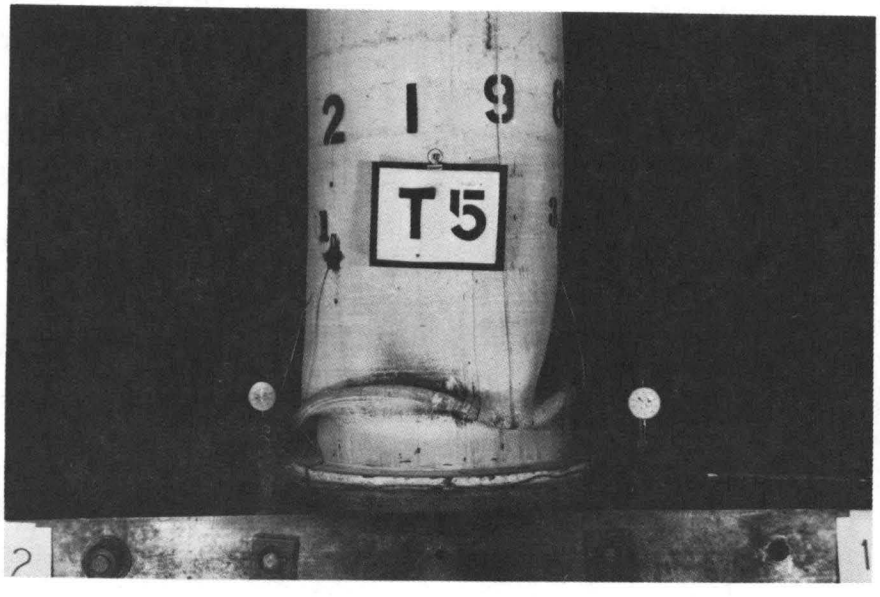

Fig. 34 Post-Buckling Deformations in T5

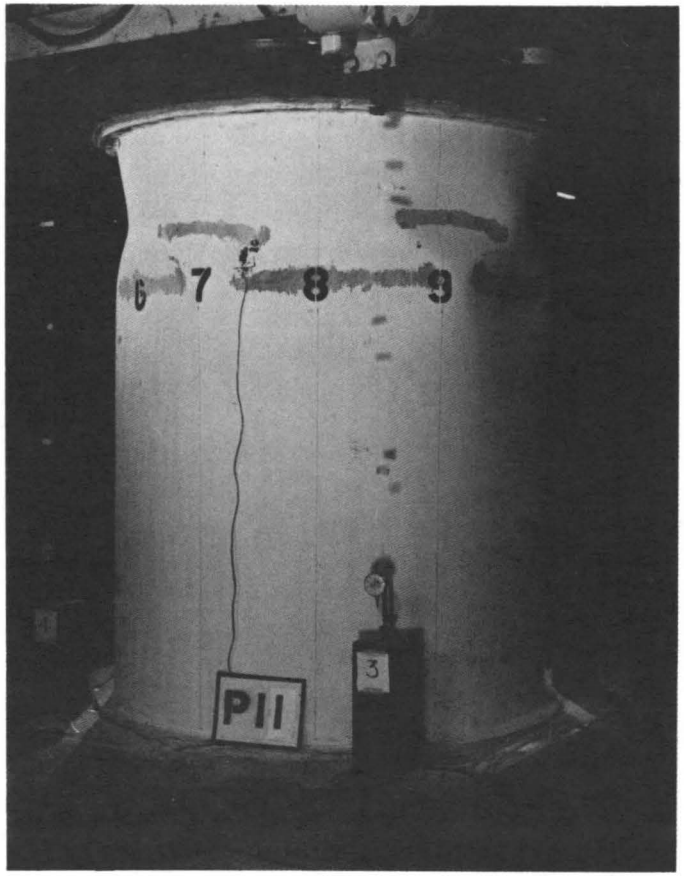

Fig. 35 Diamond-Shaped Buckles in P11

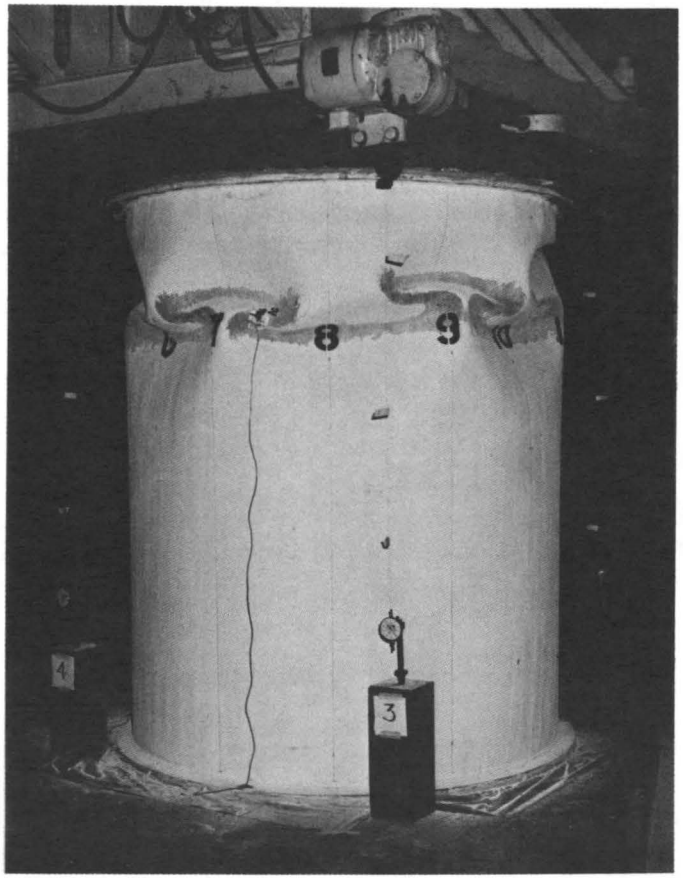

Fig. 36 Post-Buckling Deformations in P11

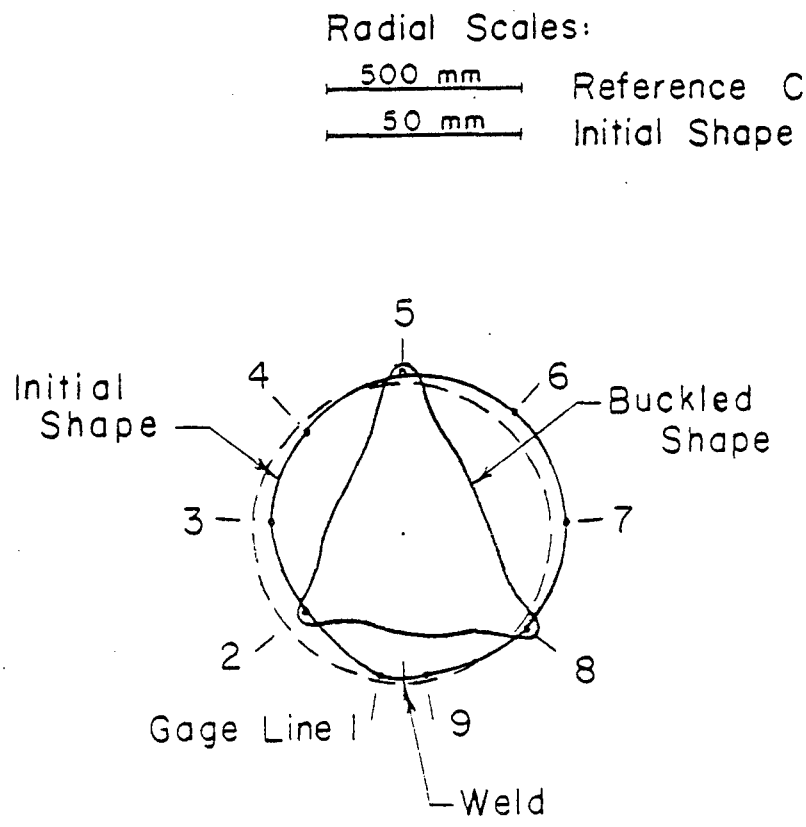

Fig. 37 Polygon Post-Buckling Pattern in T1
($D/t = 77$, $F_{ys} = 239$ MPa)

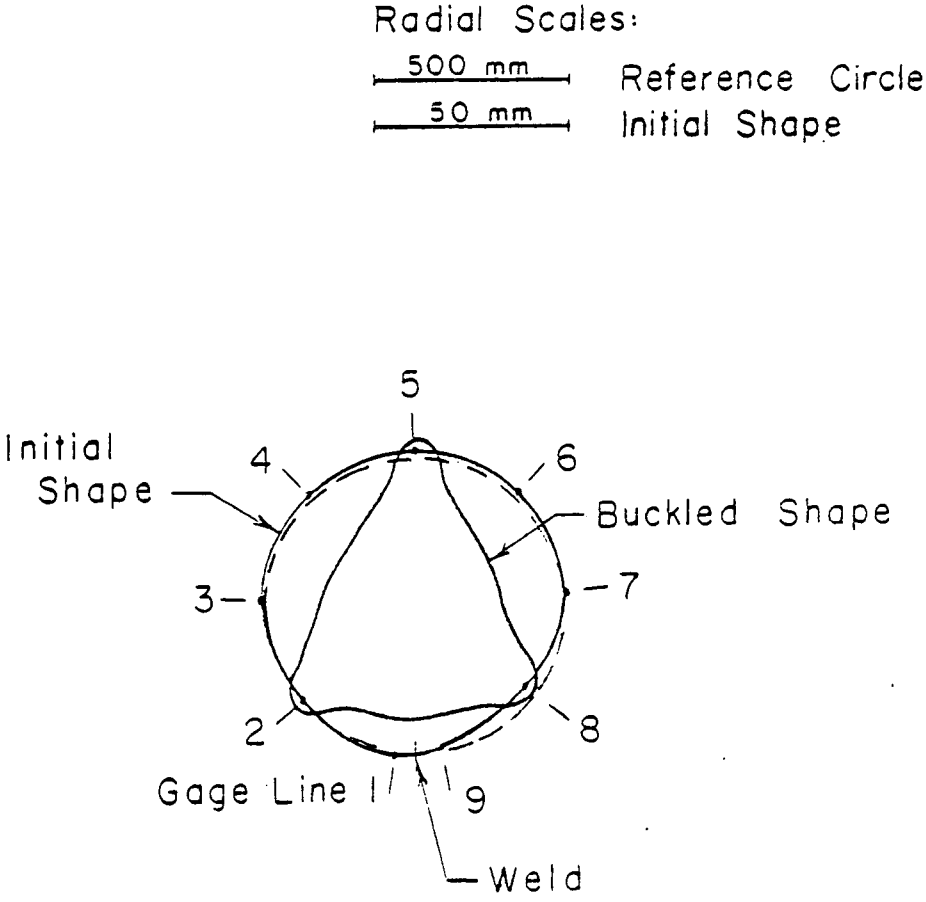

Fig. 38 Polygon Post-Buckling Pattern in T2
($D/t = 113$, $F_{ys} = 204$ MPa)

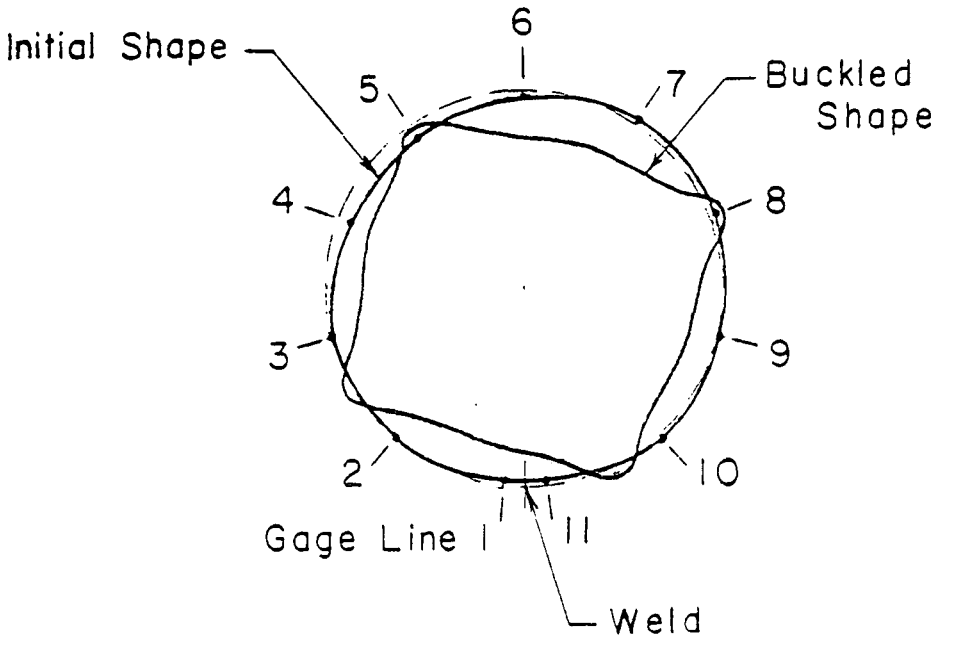

Fig. 39 Polygon Post-Buckling Pattern in T3
($D/t = 151$, $F_{ys} = 204$ MPa)

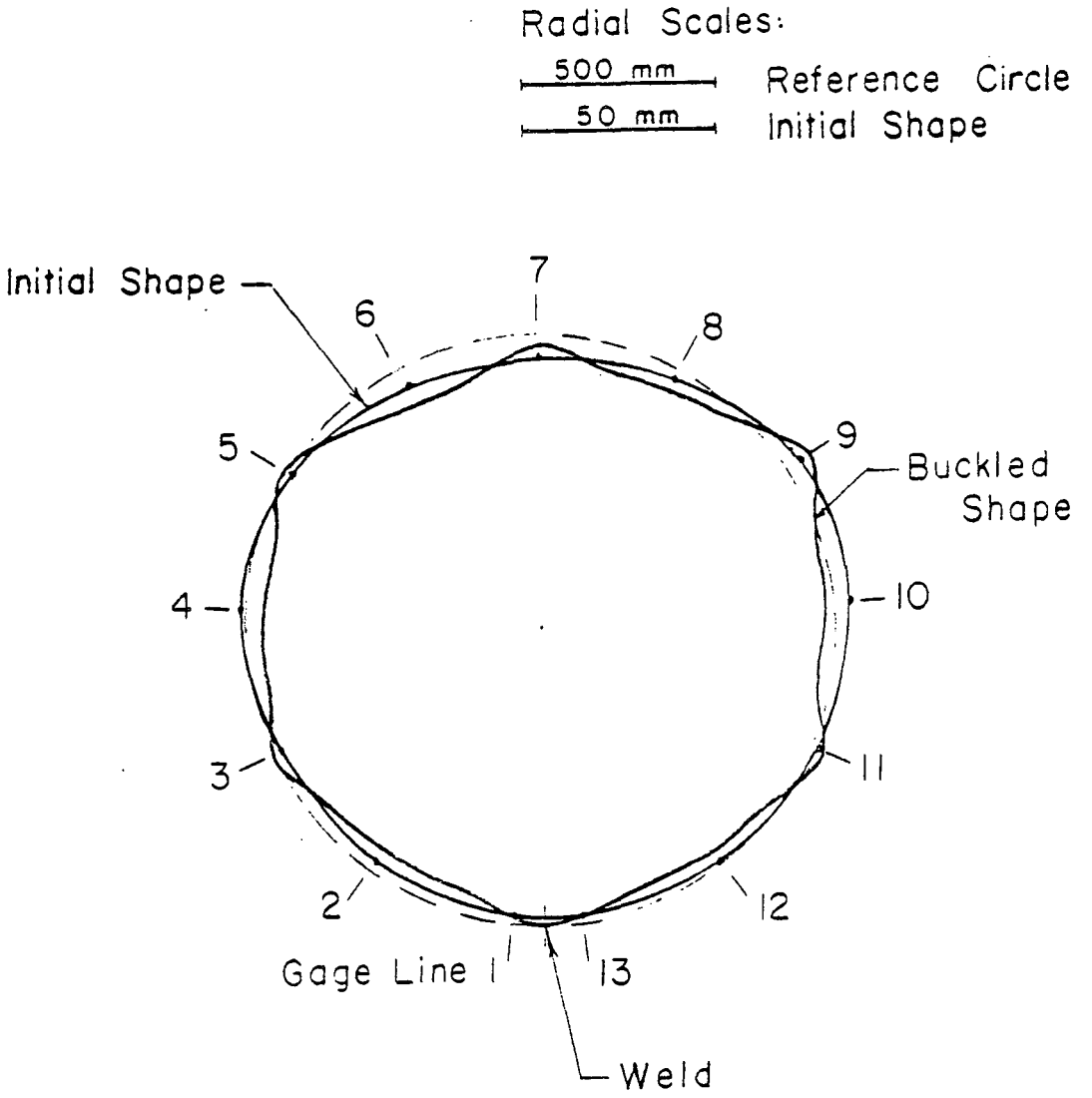

Fig. 40 Polygon Post-Buckling Pattern in T4
($D/t = 227$, $F_{ys} = 204$ MPa)

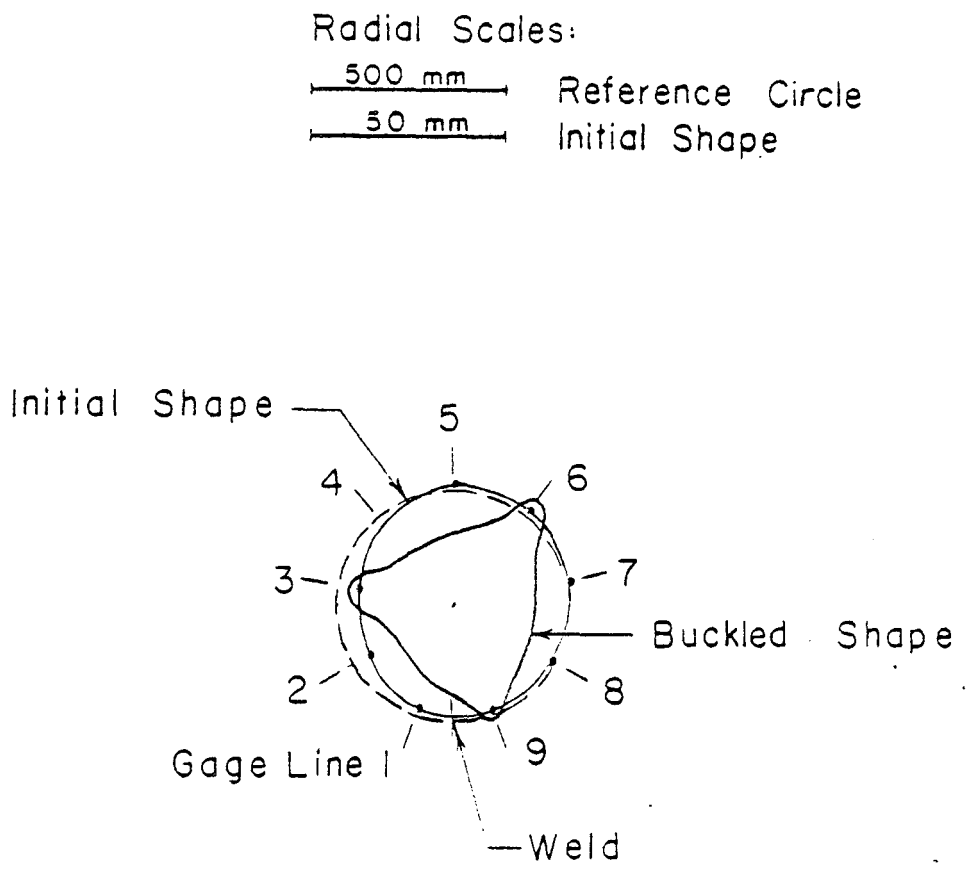

Fig. 41 Polygon Post-Buckling Pattern in T5
($D/t = 59$, $F_{ys} = 336$ MPa)

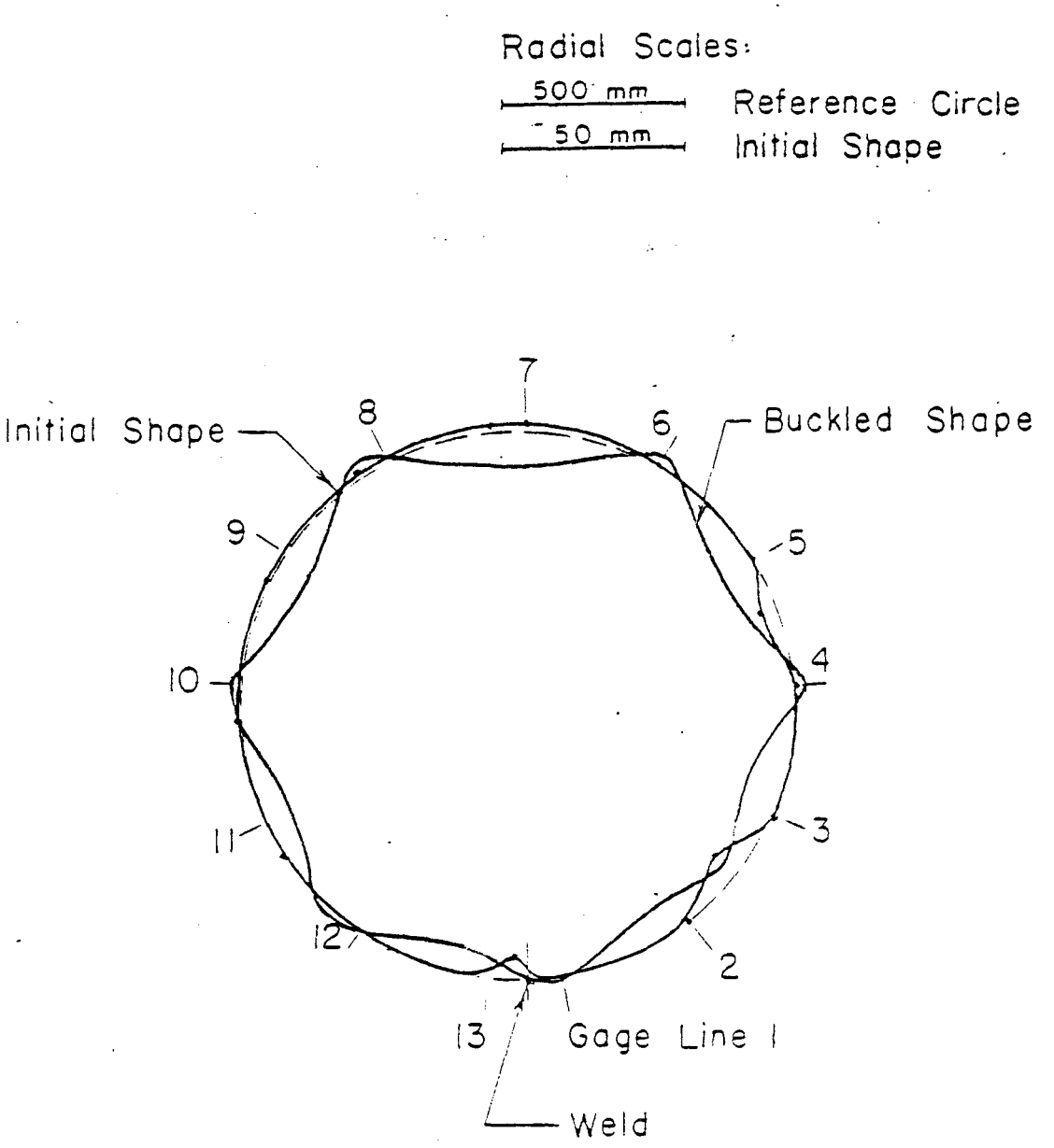

Fig. 42 Diamond-Shaped Buckling Pattern in P11
($D/t = 233$, $F_{ys} = 623$ MPa)

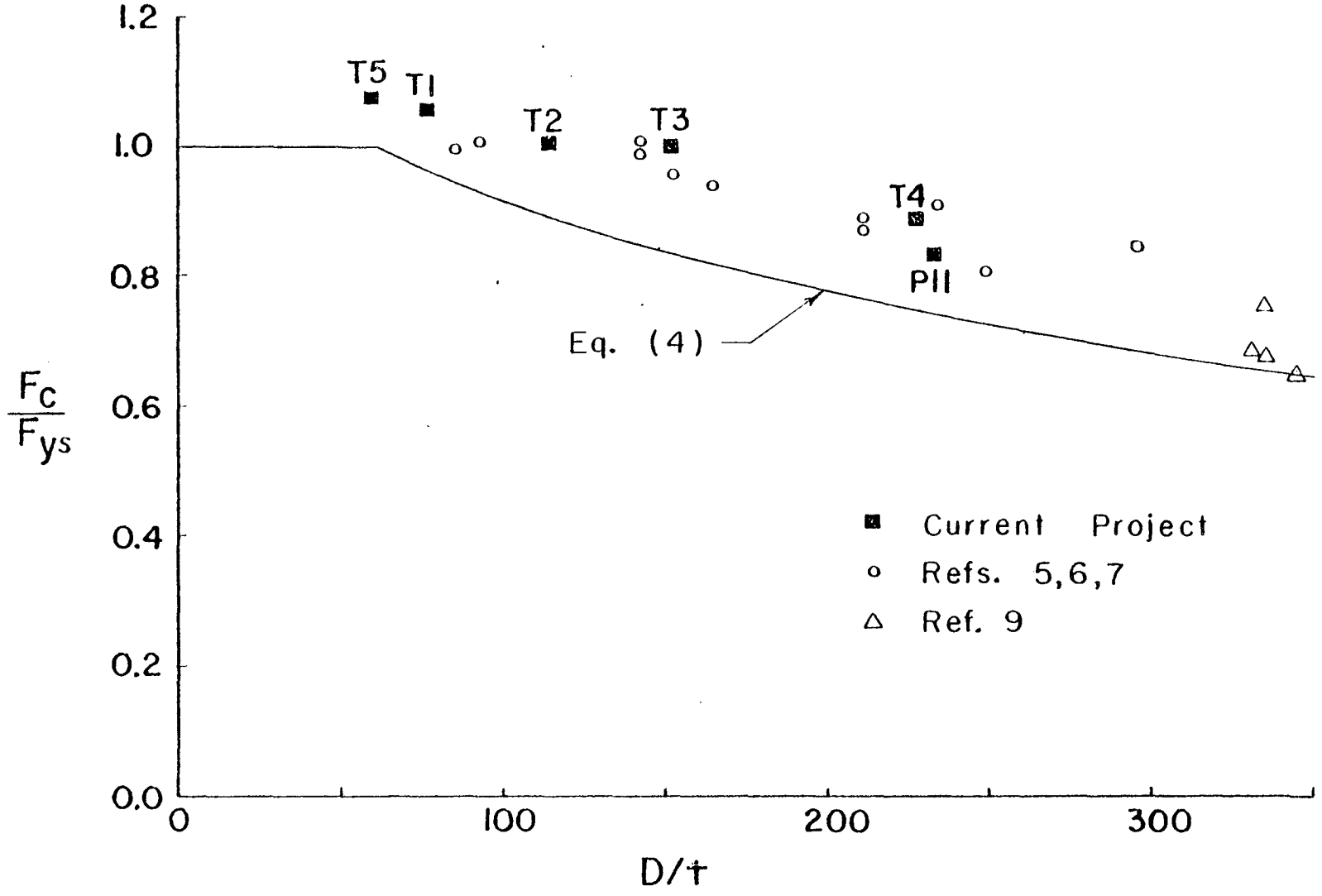

Fig. 43 Buckling Stresses vs. D/t Using F_{ys}

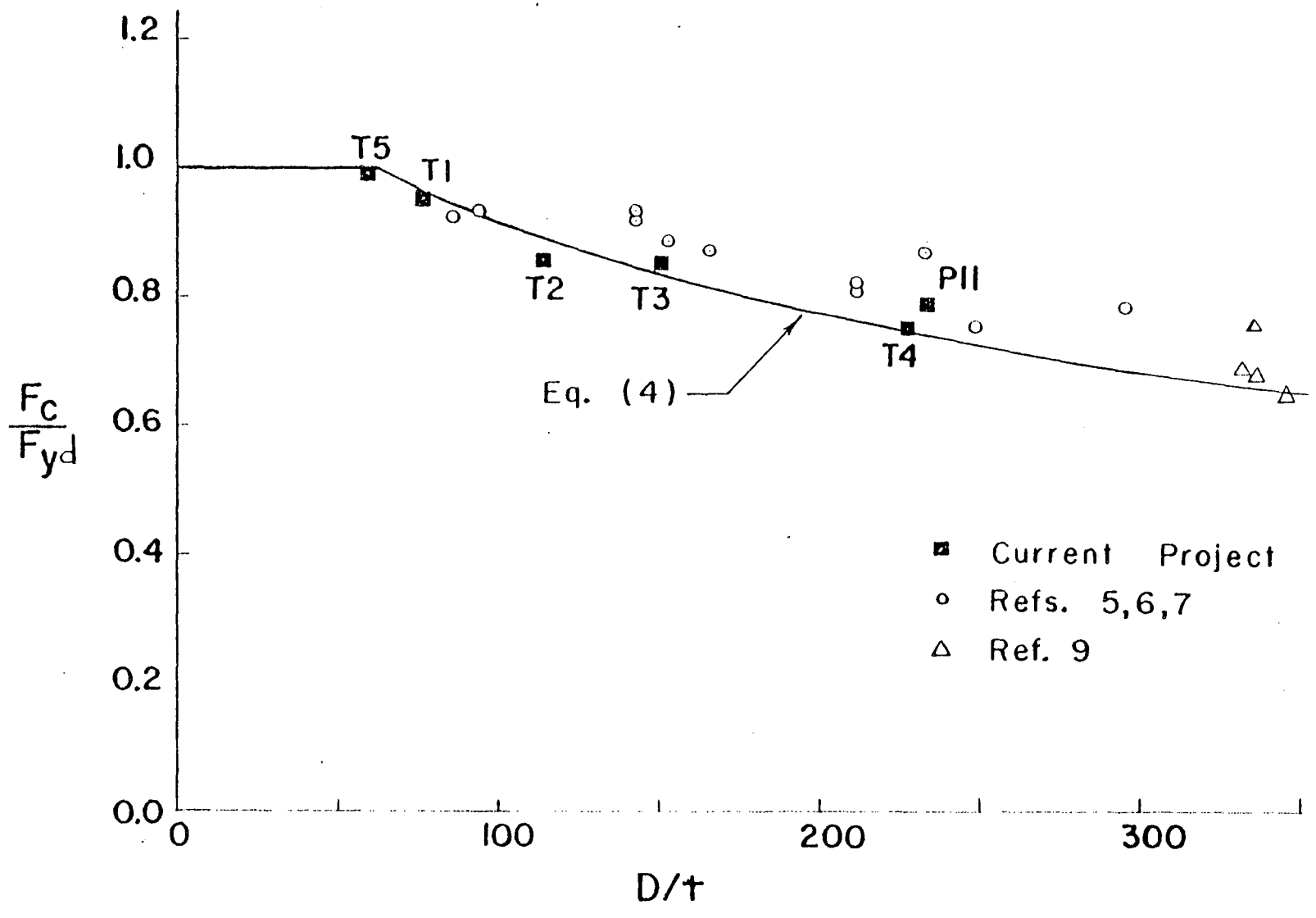

Fig. 44 Buckling Stresses vs. D/t Using F_{yd}

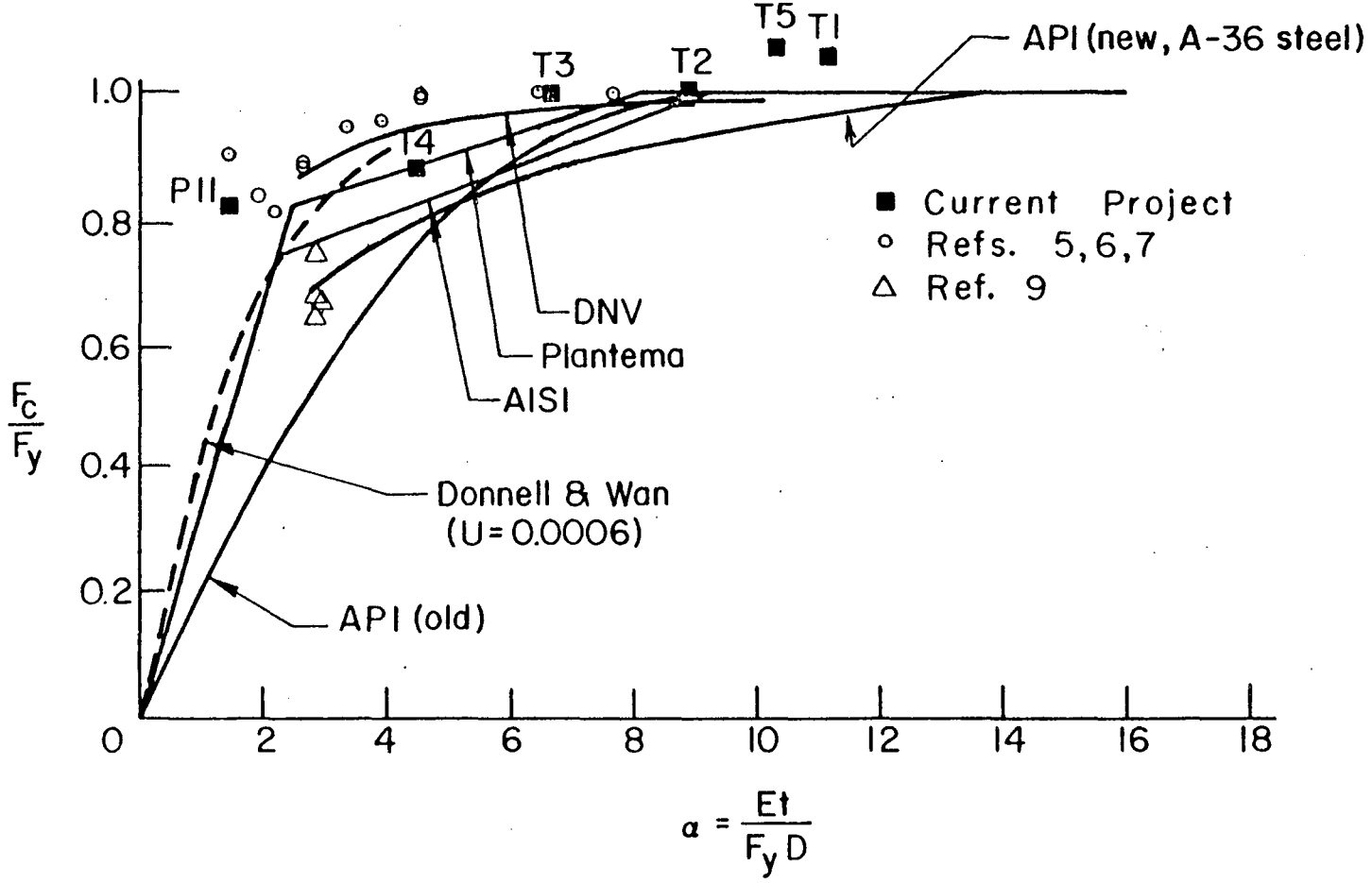

Fig. 45 Buckling Stresses vs. α

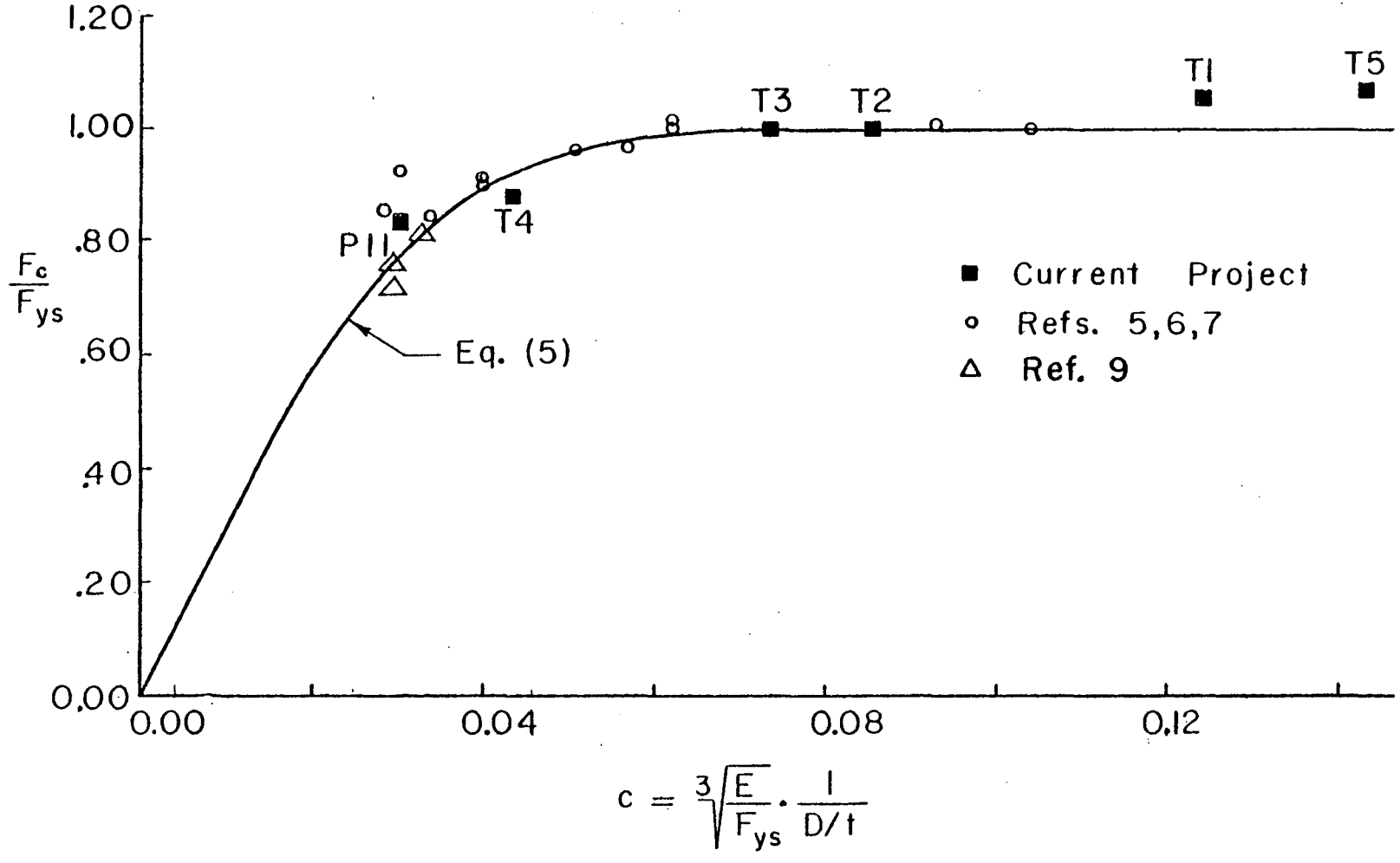

Fig. 46 Buckling Stresses vs. c